

Optimal quantum metrology protocols with erasure qubits

Michal Arieli,^{1,*} Alex Retzker,¹ and Tuvia Gefen^{1,†}

¹*Racah Institute of Physics, The Hebrew University of Jerusalem, Jerusalem 91904, Givat Ram, Israel*

(Dated: March 13, 2026)

We investigate the precision limits and optimal protocols for sensing single qubit signals in the presence of erasure noise. We study a hierarchy of precision limits achievable with metrological strategies of differing complexity, and identify the optimal protocol for each. The detectability of erasure noise is shown to lead to enhanced precision limits and simplified sensing protocols. For energy gap estimation, we demonstrate that a simple product-state continuous erasure detection strategy yields significant improvements, outperforming optimal entangled protocols even for large numbers of qubits. We show that for other single-qubit signals, quantum error correction provides a substantial advantage by correcting the dominant erasure processes, and can restore Heisenberg-limited precision in certain erasure configurations. As a byproduct of our analysis, we find erasure-conversion schemes for qubits subject to thermal noise that attain the corresponding ultimate precision limits.

Introduction—Several quantum technologies rely on precise sensing of single-qubit signals in the presence of noise. Examples include energy gap estimation in atomic clocks [1–6], Zeeman shift estimation in magnetometers [7–10], nano-NMR [11–14], and Rabi frequency estimation [15–17]. In the absence of noise, optimal protocols typically exploit entanglement to achieve quantum enhanced precision, where the fundamental limit in frequency estimation is known as the Heisenberg limit (HL) [18]. Noise significantly degrades the precision and prevents achieving HL [19, 20]. In recent years, there has been a tremendous progress in finding optimal sensing protocols and precision bounds for these problems [21–32]. Several methods of noise mitigation and correction for quantum metrology were devised, yet for most relevant cases, e.g., amplitude damping noise, dephasing, and coupling to a thermal bath, Heisenberg scaling cannot be retrieved [20, 23–25].

In many physical systems, the main noise mechanism can be engineered or converted to an erasure noise, which is a detectable error [33–41]. This feature has already proven highly valuable in quantum computing, where erasure conversion substantially increases error correction thresholds and improves noisy performance [33, 34, 42, 43]. For quantum metrology, recent works have also demonstrated improved performance in the presence of erasure noise or via erasure conversion [44–51]. However, a systematic study of precision bounds and optimal protocols given this noise is missing. In particular, it would be instructive to understand how the detectability of these errors improve the sensitivity limits and simplify the optimal protocols.

In this work, we address these questions by investigating the precision limits for estimating single-body signals of erasure qubits using metrological strategies of varying complexity. We find that the detectability of erasure noise gives rise to several key features that are the main results of this Letter. For certain signals, such as Rabi-frequency estimation, this detectability leads to substan-

tially improved precision limits. In these cases, quantum error correction (QEC) can correct the dominant erasure noise and provide a significant metrological advantage, reaching HL in some erasure configurations. For energy gap estimation, the metrological gain is more limited; however, this detectability can provide enhancement with simplified protocols. In this case, the optimal strategy in the asymptotic limit involves only spin squeezing [52]. We further show that a continuous erasure detection protocol applied to product states yields a significant improvement, outperforming optimal passive entangled strategies for systems of up to ~ 100 qubits. These results are also applied for qubits subject to thermal noise, demonstrating that erasure conversion followed by spin squeezing is asymptotically optimal.

Erasure qubit—We consider a qubit probe, and denote its computational basis as $\{|1\rangle, |2\rangle\}$. The Hamiltonian acting on this probe is given by $H = \omega G$, where ω is the parameter we want to estimate and G is a generic single qubit operator, and thus takes the form of $G = \vec{n} \cdot \vec{\sigma}$, where \vec{n} is a unit vector and $\vec{\sigma}$ is the vector of Pauli matrices. The qubit is subject to an erasure noise; that is, a noise that maps the qubit subspace into auxiliary states, denoted by $\{|e_i\rangle\}_{i=1}^k$. More concretely, we consider a time evolution given by the following Lindblad master equation:

$$\dot{\rho} = -i[\omega G, \rho] + \sum_{i,j} \left(L_{i,j} \rho L_{i,j}^\dagger - \frac{1}{2} \{L_{i,j}^\dagger L_{i,j}, \rho\} \right), \quad (1)$$

where $L_{i,j} = \sqrt{\gamma_{i,j}} |e_j\rangle\langle i|$ are the erasure jump operators that correspond to a decay from the qubit state $|i\rangle$ ($i = 1, 2$) to the erasure states $|e_j\rangle$, and $\gamma_{i,j}$ are the decay rates. This setting is illustrated in Fig. 1 (a). We denote by $\mathcal{E}(t)$ the quantum channel given by evolving the qubit under this Lindblad equation.

Protocol classes and their precision limits—Given this erasure qubit setting, we consider estimating the parameter ω and organize quantum metrology strategies into classes of varying complexity. For each class of

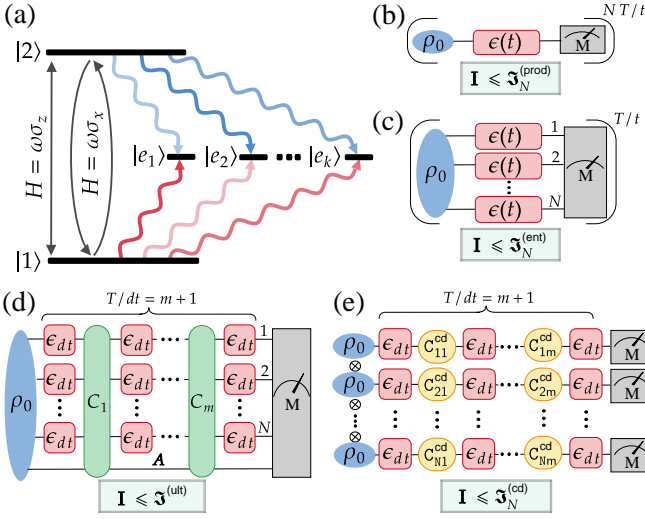


Figure 1: (a) Schematic of the erasure qubit. Each level of the qubit probe $|i\rangle$ ($i = 1, 2$) can decay to an erasure state $|e_j\rangle$ with rate $\gamma_{i,j}$. (b) Product protocols (class (i)): initializing and measuring each qubit individually. (c) Entangled protocols (class (ii)): includes also ancilla-free entangled states and measurements. (d) Sequential protocols (class (iii)): the most general entangled and adaptive strategies, in which we allow any quantum fast control and arbitrary entanglement of the probes with ancillas. (e) Continuous erasure detection protocols (class (iv)): the qubits are initialized into a product state and subjected to restricted controls, allowing for erasure detection and a fast reset. The achievable precision in classes (i)–(iv) is bounded by $\mathfrak{J}_N^{(\text{prod})}$, $\mathfrak{J}_N^{(\text{ent})}$, $\mathfrak{J}_N^{(\text{ult})}$ (asymptotically in large NT), and $\mathfrak{J}_N^{(\text{cd})}$, respectively.

strategies, we define the associated precision limit as the optimal precision achievable within that class.

In general, these precision limits rely on the quantum (classical) Cramér-Rao bounds, which state that $\Delta\omega \geq I^{-1/2}$ ($\Delta\omega \geq I_C^{-1/2}$), where I (I_C) corresponds to the quantum (classical) Fisher information. The classical Fisher information (CFI) can be calculated directly from the probability distribution of the outcomes, $\{p_i(\omega)\}_i$: $I_C = \sum_i (\partial_\omega p_i)^2 / p_i$. Similarly the quantum Fisher information (QFI) can be calculated directly from the density matrix of the probe, $\rho(\omega)$ [53, 54]: $I(\rho) = \sum_{j,k} \frac{2}{p_j + p_k} |\langle \psi_j | \partial_\omega \rho | \psi_k \rangle|^2$, where p_k are the non-zero eigenvalues of the density matrix ρ and $|\psi_k\rangle$ are the corresponding eigenstates.

Assuming that we have N erasure qubits that evolve according to Eq. 1, and a total time T , we consider the different classes of metrological strategies that are illustrated in Fig. 1.

The simplest strategy class is (i) where the N qubit

probes are initialized in a product state and allowed to evolve freely for a duration t , after which a measurement is performed. This procedure is repeated T/t times. The maximal QFI achievable within this class is denoted by $\mathfrak{J}_N^{(\text{prod})}$. This bound is attained when both the product initial state and t are optimized. It is well established that in the noiseless case $\mathfrak{J}_N^{(\text{prod})} \propto NT^2$, while in the noisy case it typically scales as $\mathfrak{J}_N^{(\text{prod})} \propto NT$ [20, 21, 28].

The second strategy class (ii) consists of *entangled* (ancilla-free) strategies. These extend class (i) by allowing for a general entangled input state and measurement. The optimal QFI achievable within this class is denoted by $\mathfrak{J}_N^{(\text{ent})}$. In the noiseless case, $\mathfrak{J}_N^{(\text{ent})} \propto N^2T^2$ while in the presence of noise, $\mathfrak{J}_N^{(\text{ent})} \propto NT$ [20, 21, 28].

We further define $\mathcal{I}_N^{(\text{prod})}$ and $\mathcal{I}_N^{(\text{ent})}$ as the maximal QFI within these classes when only the input state is optimized. For class (i) this can be calculated efficiently using the single-qubit extended-channel QFI (ECQFI) technique, whereas for class (ii) the calculation is in general more complex. Specifically, it can be calculated with an iterative see-saw (ISS) method [32, 55, 56], while the ECQFI method is not necessarily tight. Calculation of this $\mathcal{I}_N^{(\text{ent})}$ might be also intractable in the large N limit.

The most general strategy class (iii) consists of sequential protocols, in which we allow any possible sequential control, any input state and any number of noiseless ancillas. The optimal QFI within this class in the asymptotic limit of large T (or N) is denoted by $\mathfrak{J}_N^{(\text{ult})}$. It represents the ultimate precision bound, since it includes optimization over all possible protocols. $\mathfrak{J}_N^{(\text{ult})}$ can be easily calculated using the sequential ECQFI bound that was developed in Refs. [23–25]. It was further shown in Refs. [23–25] that $\mathfrak{J}_N^{(\text{ult})} \propto N^2T^2$ iff $G \notin \text{span} \left\{ \mathbb{1}, L_{i,j}, L_{i,j}^\dagger, L_{i,j}^\dagger L_{k,m} \right\}_{i,j,k,m}$, where G and $\{L_{i,j}\}$ are the Hamiltonian and jump operators in Eq. 1 respectively. Otherwise, $\mathfrak{J}_N^{(\text{ult})} \propto NT$.

These classes of metrological strategies satisfy (i) \subseteq (ii) \subseteq (iii), and thus the corresponding QFI bounds satisfy $\mathfrak{J}_N^{(\text{prod})} \leq \mathfrak{J}_N^{(\text{ent})} \leq \mathfrak{J}_N^{(\text{ult})}$. This chain of inequalities is true for every N and T .

We study in this Letter another class of protocols (iv), which is particularly relevant to erasure noise: continuous erasure detection (CD). In this strategy class, the input state can be any product state and the erasure levels are being continuously monitored [57–59]. A continuous feedback and control is applied based on the erasure detection outcomes, e.g., the qubit is reset following detection events. This strategy is clearly still limited by $\mathfrak{J}_N^{(\text{ult})}$. However, we show that it can be considerably better than strategy class (i) (optimal product state), and furthermore in some cases it also outperforms strategy class (ii) (optimal entangled states protocols) up to a large N .

For erasure qubits, this hierarchy of precision limits

strongly depends on G and on the erasure decay rates $\{\gamma_{i,j}\}$. In what follows we explore these limits and the optimal protocols. We split into cases of $G = \sigma_z$, and $G \perp \sigma_z$.

Precision limits for $G = \sigma_z$ — For $G = \sigma_z$ the gain obtained from entangled and sequential strategies is quite limited. We show this by calculating the precision bounds of the different strategies. For convenience, we denote $\Gamma_1 := \sum_{j=1}^k \gamma_{1,j}$, $\Gamma_2 := \sum_{j=1}^k \gamma_{2,j}$, and remark that in this case all bounds depend solely on these sums.

We begin with the ultimate limit, given by [23–25]:

$$\mathcal{J}^{(\text{ult})} = 4 \min_h \left[\left(\frac{NT}{dt} \right) \|\alpha\| + \left(\frac{NT}{dt} \right)^2 \|\beta\| \left(\|\beta\| + 2\sqrt{\|\alpha\|} \right) \right],$$

where $\alpha = (\dot{\mathbf{K}}_{dt} - ih\mathbf{K}_{dt})^\dagger (\dot{\mathbf{K}}_{dt} - ih\mathbf{K}_{dt})$, $\beta = i\mathbf{K}_{dt}^\dagger (\dot{\mathbf{K}}_{dt} - ih\mathbf{K}_{dt})$, and \mathbf{K}_{dt} is a vector of the Kraus operators of the infinitesimal evolution channel $\mathcal{E}(dt)$. Applying this to our case (Eq. 1 with $G = \sigma_z$) leads to

$$\mathcal{J}^{(\text{ult})} = \frac{16NT}{(\sqrt{\Gamma_1} + \sqrt{\Gamma_2})^2}. \quad (2)$$

A derivation of this bound is provided in the supplemental [60]. Eq. 2 is the ultimate precision limit and thus establishes that Heisenberg scaling with N and T cannot be achieved in this case.

Let us compare this bound to the QFI of the simplest strategy: optimal product states ($\mathcal{J}_N^{(\text{prod})}$). We calculate $\mathcal{I}_N^{(\text{prod})}$ using the single-qubit ECQFI bound [20, 61, 62], which optimizes the QFI for a quantum channel $\mathcal{E}(t)$ over all input states. The bound reads $\mathcal{I}_1(\mathcal{E}(t)) = \min_h \|\alpha\|$, with $\alpha = (\dot{\mathbf{K}}_t - ih\mathbf{K}_t)^\dagger (\dot{\mathbf{K}}_t - ih\mathbf{K}_t)$ and \mathbf{K}_t is the vector of Kraus operators of $\mathcal{E}(t)$. Applying this bound to our problem yields:

$$\mathcal{J}_N^{(\text{prod})} = \max_t \frac{16tNT}{\left(e^{\frac{\Gamma_1 t}{2}} + e^{\frac{\Gamma_2 t}{2}} \right)^2} \approx \begin{cases} \frac{2.47}{\Gamma_{\max}} NT & \Gamma_{\min} = 0 \\ \frac{4}{e\Gamma_{\max}} NT & \Gamma_{\min} = \Gamma_{\max}, \end{cases} \quad (3)$$

where $\Gamma_{\min, \max}$ are the extrema of $\{\Gamma_1, \Gamma_2\}$, and the optimal measurement time, t_{opt} , is obtained numerically. This bound is saturated without the usual requirement for ancilla entanglement. It is achieved by the single qubit state $|\psi_{\text{opt}}\rangle = \sqrt{p_{\text{opt}}}|1\rangle + \sqrt{1-p_{\text{opt}}}|2\rangle$ with $p_{\text{opt}} = [1 + \tanh \frac{t_{\text{opt}}}{4}(\Gamma_1 - \Gamma_2)]/2$. Comparing to the ultimate bound we observe $2.7 \leq \mathcal{J}^{(\text{ult})}/\mathcal{J}_N^{(\text{prod})} \leq 6.47$, where the maximal metrological gain is obtained for $\Gamma_{\min} = 0$, and the minimal is for $\Gamma_{\min} = \Gamma_{\max}$. This comparison is presented in Fig. 2.

It is now desirable to understand which protocols attain $\mathcal{J}^{(\text{ult})}$ and how much improvement over $\mathcal{J}_N^{(\text{prod})}$ can be obtained using entanglement and CD strategies. Let us first explore the performance of optimal entangled states (strategy class (ii)). We show that this strategy is optimal in the asymptotic limit:

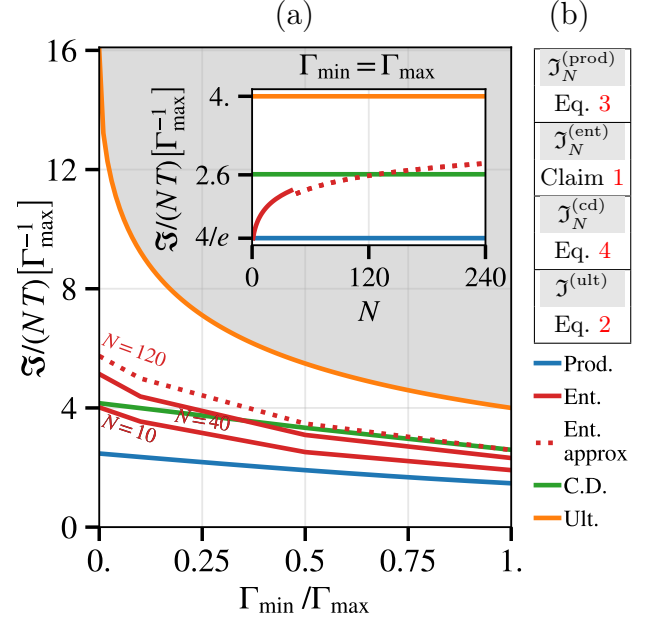


Figure 2: Hierarchy of precision limits for $G = \sigma_z$. (a) Main plot: optimal QFI rate with different strategies as a function of $\Gamma_{\min}/\Gamma_{\max}$. This figure presents the gap between the ultimate limit (orange line), optimal product strategies (blue line) and optimal entangled strategies for different N (red solid and dotted lines correspond to exact and approximate values respectively [60]). Continuous erasure detection (green line) outperforms entangled strategies up to a certain N , where this crossover depends on the decay rates. Inset: optimal QFI with the different strategies as a function of N for the symmetric case $\Gamma_{\max} = \Gamma_{\min}$. Continuous erasure detection outperforms entangled strategies up to $N \sim 120$. (b) Summary of the precision limits achieved with the different metrological strategies for $G = \sigma_z$.

Claim 1. $\lim_{N \rightarrow \infty} \mathcal{J}_N^{(\text{ent})} = \mathcal{J}^{(\text{ult})}$ for any Γ_1, Γ_2 , and this saturation is achieved using an optimal spin squeezed state and optimizing over its evolution time t .

The case of $\Gamma_1 = \Gamma_2$ was proven in Ref. [63], we generalize this proof in the supplemental material to any Γ_1, Γ_2 [60]. This is done by calculating the error propagation approximation of the QFI and showing that for optimal spin squeezing it converges to $\mathcal{J}^{(\text{ult})}$. The orientation of the optimal spin squeezed states depends on Γ_1, Γ_2 , where for unequal decay rates its center is shifted away from the equator.

Claim 1, however, corresponds only to the asymptotic $N \rightarrow \infty$ limit. To examine the performance in the finite N regime, we plot $\mathcal{J}_N^{(\text{ent})}$ as a function of N in Fig. 2. It can be observed that, while this strategy is asymptotically optimal, its convergence to $\mathcal{J}^{(\text{ult})}$ is slow. We find that the optimal entangled states correspond to spin

squeezed states for $N \geq 40$. These numerical calculations are done using iterative see-saw (ISS) methods [32, 55, 56].

Let us now analyze the performance of CD protocols (strategy class (iv)), where we continuously measure the erasure states, detecting whether a decay occurred. A feedback and control is implemented on the qubits based on the erasure detection outcomes. Clearly, if an erasure is detected, the optimal control is to reset the qubit to an optimal input state. If no erasure was detected, we let the qubit evolve freely up to τ , after which an optimal measurement is performed. Optimizing this strategy gives [60]

$$\mathcal{J}_N^{(\text{cd})} = \max_{\tau} \frac{16\tau^2 NT}{\left(\sqrt{\int_0^{\tau} e^{\Gamma_1 t} dt} + \sqrt{\int_0^{\tau} e^{\Gamma_2 t} dt}\right)^2}. \quad (4)$$

$$\approx \begin{cases} \frac{4.16}{\Gamma_{\min}} NT & \Gamma_{\min} = 0 \\ \frac{2.6}{\Gamma_{\max}} NT & \Gamma_{\min} = \Gamma_{\max}. \end{cases}$$

This bound is shown in Fig. 2 for different $\Gamma_{\min}, \Gamma_{\max}$. $\mathcal{J}_N^{(\text{cd})}$ improves on $\mathcal{J}_N^{(\text{prod})}$ by a factor of 1.68–1.76, a gain that results from resetting the state whenever an erasure is detected. To better appreciate the performance of this strategy, we compare its QFI to that of the optimal entangled strategy for finite N . We observe that in the symmetric case ($\Gamma_{\min} = \Gamma_{\max}$), $\mathcal{J}_N^{(\text{cd})}$ outperforms $\mathcal{J}_N^{(\text{ent})}$ up to $N \approx 120$ qubits (Fig. 2 inset). Therefore, although the CD strategy is asymptotically inferior to the optimal entangled strategy as $N \rightarrow \infty$, it considerably outperforms it in the small N regime. This comparison highlights the effectiveness of CD strategies. For asymmetric decay, $\Gamma_{\min} < \Gamma_{\max}$, the crossover between $\mathcal{J}_N^{(\text{cd})}$ and $\mathcal{J}_N^{(\text{ent})}$ occurs at smaller N (see Fig. 2). We anticipate that combining entanglement with CD can lead to further improvement. While we leave it to future work, we show in the supplemental an example of CD with two-qubit entanglement that achieves in the symmetric erasure configuration a QFI of $2.72NT/\Gamma_{\max}$, outperforming the product state CD bound.

Finally, we revisit Claim 1 and remark that it has applications to other noise channels that can be converted to erasure noise: it can be used to construct asymptotically optimal strategies for these noises via erasure conversion. Consider qubits subject to thermal noise. It is well established that $\mathcal{J}^{(\text{ult})}$ in this case is identical to the erasure qubit bound of Eq. 2, where Γ_1, Γ_2 correspond to the decay and excitation rates [23]. These noises can be converted to erasure noise using the following code space $\{|0\rangle_L = |11\rangle, |1\rangle_L = |22\rangle\}$, which constitutes a logical erasure qubit [60]. Applying Claim 1 to this logical erasure qubit, we get that an optimal logical spin squeezing with this code space attains $\mathcal{J}^{(\text{ult})}$. This protocol is a simpler alternative to other protocols in the literature that rely on conversion to dephasing noise [28].

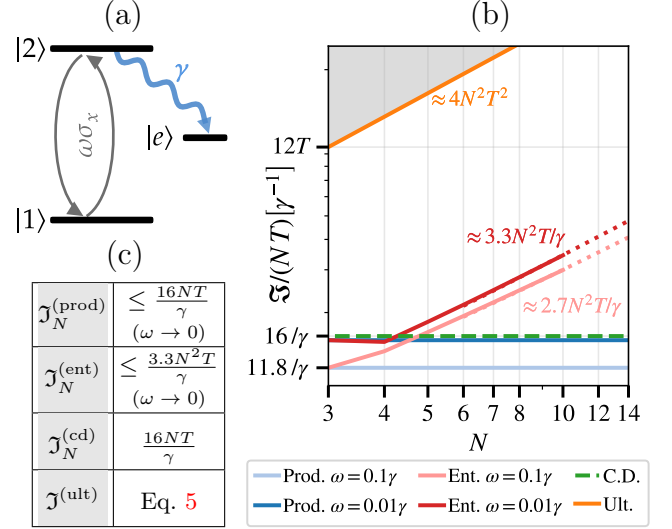


Figure 3: Hierarchy of precision limits for $G = \sigma_x$ under single erasure noise, as sketched in (a). (b) Optimal QFI rate as a function of N . The optimal product strategies for $\omega = 0.1\gamma$ and 0.01γ (bright and dark blue lines, respectively) approach $16/\gamma$ in the limit $\omega \rightarrow 0$. In contrast, the optimal continuous detection strategy (dashed green line) attains this value for any ω . While these protocols are limited to SQL scaling, the optimal entangled strategies ($\omega = 0.1\gamma, 0.01\gamma$, given by the pink, red lines respectively) achieve a Heisenberg scaling in N , but not in T . The ultimate bound (orange line) is the noiseless HL. (c) Summary of the precision limits.

Precision limits for $G \perp \sigma_z$ — For $G = \sigma_x$, and equivalently any other G in the $\sigma_x - \sigma_y$ plane, the precision limits with the different protocols are markedly different. In this setting, the gain from optimal entangled and sequential strategies can be substantially larger, and for extreme asymmetric erasure noise HL is in theory achievable.

For a general erasure configuration $\mathcal{J}^{(\text{ult})}$ is given by

$$\frac{2NT}{\sum_{j=1}^k \min\{\gamma_{1,j}, \gamma_{2,j}\}} \leq \mathcal{J}^{(\text{ult})} \leq \frac{4NT}{\sum_{j=1}^k \min\{\gamma_{1,j}, \gamma_{2,j}\}},$$

$$\mathcal{J}^{(\text{ult})} = 4N^2T^2 \quad (\text{if } \forall j \min\{\gamma_{1,j}, \gamma_{2,j}\} = 0). \quad (5)$$

This bound represents an effective decay rate of $\sum_{j=1}^k \min\{\gamma_{1,j}, \gamma_{2,j}\}$. In the asymmetric erasure regime, i.e., for all j , $\gamma_{1,j} \ll \gamma_{2,j}$ or $\gamma_{2,j} \ll \gamma_{1,j}$, this bound is significantly larger than the corresponding thermal noise bound [64] as well as the erasure $G = \sigma_z$ bound (Eq. 2). Furthermore, in the extreme asymmetric case where $\min\{\gamma_{1,j}, \gamma_{2,j}\} = 0$ (for every j) the decay can be fully corrected using QEC, allowing the recovery of the noiseless HL: $\mathcal{J}^{(\text{ult})} = 4N^2T^2$.

This HL is attainable using the following QEC

code $\{|0_L\rangle = |+\rangle|+\rangle, |1_L\rangle = |-\rangle|-\rangle\}$, where $|\pm\rangle = \sqrt{1/2}(|0\rangle \pm |1\rangle)$. Preparing the N qubits in the logical GHZ state $\sqrt{1/2}(|0_L\rangle^{N/2} + |1_L\rangle^{N/2})$ and applying a continuous QEC restores the noiseless HL [15, 16, 49]. In general, using this QEC code yields an effective logical Hamiltonian $H_L = 2\omega(|0_L\rangle\langle 0_L| - |1_L\rangle\langle 1_L|)$ together with a logical dephasing rate $\sum_{j=1}^k \min\{\gamma_{1,j}, \gamma_{2,j}\}$. Consequently, whenever the HL cannot be reached (i.e., $\min\{\gamma_{1,j}, \gamma_{2,j}\} > 0$), this QEC code attains a QFI of $\frac{2NT}{\sum_{j=1}^k \min\{\gamma_{1,j}, \gamma_{2,j}\}}$, which matches the lower bound of Eq. 5. This QFI is achieved asymptotically by preparing an optimal logical spin squeezed state with this QEC code [28, 60].

In most erasure configurations, however, $\mathfrak{J}^{(\text{ult})} > \frac{2NT}{\sum_{j=1}^k \min\{\gamma_{1,j}, \gamma_{2,j}\}}$, indicating that alternative QEC codes are required to saturate $\mathfrak{J}^{(\text{ult})}$. Consider a single erasure state scenario with $\gamma_1, \gamma_2 > 0$ and without loss of generality $\gamma_1 \leq \gamma_2$, then $\mathfrak{J}^{(\text{ult})} = \frac{4NT}{\gamma_1}$, which corresponds to the upper bound of Eq. 5. This $\mathfrak{J}^{(\text{ult})}$ is saturable asymptotically with the following “zero signal, zero noise” code: $\{|0_L\rangle = |\epsilon_+\rangle|0\rangle_a, |1_L\rangle = |\epsilon_-\rangle|1\rangle_a\}$, where $|0/1\rangle_a$ denotes noiseless ancillary states, $|\epsilon_\pm\rangle = \epsilon|1\rangle \pm \sqrt{1-\epsilon^2}|2\rangle$, and $\epsilon \rightarrow 0$, which is the limit of vanishing signal and vanishing noise. A derivation of the optimality of these QEC codes, along with further numerical calculations of $\mathfrak{J}^{(\text{ult})}$ in general erasure configurations are provided in the supplemental [60].

To illustrate the significant gain of QEC protocols, let us compare $\mathfrak{J}^{(\text{ult})}$ to the optimal product state QFI, $\mathfrak{J}_N^{(\text{prod})}$. For simplicity, we restrict ourselves to the simplest case of a single erasure decay from $|2\rangle$, i.e., $\gamma_1 = 0, \gamma := \gamma_2 > 0$, as illustrated in Fig. 3 (a). While QEC protocols achieve HL, we find that $\mathfrak{J}_N^{(\text{prod})} \leq 16NT/\gamma$, where equality is achieved only in the limit of $\omega \rightarrow 0$. In this limit, $\mathfrak{J}_N^{(\text{prod})}$ is obtained by initializing every qubit to $|1\rangle$, which becomes a noiseless state as $\omega \rightarrow 0$. Given that $\omega \ll \gamma$, we can adiabatically eliminate the fast decaying state $|2\rangle$, such that the dynamics is described by an effective erasure decay from $|1\rangle$ with decay rate of $\gamma_{\text{eff}} = 4\omega^2/\gamma$. This effective erasure dynamics then accounts for a QFI of $16NT/\gamma$ [60, 65, 66].

We further study the performance of CD protocols, and find that they also fall substantially short of $\mathfrak{J}^{(\text{ult})}$ in the asymmetric erasure regime. Focusing again on the case of a single erasure decay, we find that the optimal strategy is to reset the state only after erasure detection, so that all the information is encoded in the decay times. The QFI of this protocol can be calculated analytically and is equal to $\mathfrak{J}_N^{(\text{cd})} = 16NT/\gamma$. It thus reaches the same limit as $\mathfrak{J}_N^{(\text{prod})}$, but does so for any ω , not only in the regime of $\omega \ll \gamma$.

Lastly, we discuss the entangled strategy and $\mathfrak{J}_N^{(\text{ent})}$. In the limit of large N this strategy attains Heisenberg scaling with N , but not with T , since Heisenberg scaling

with T requires sequential QEC. From numerical simulations, we obtain that for large enough N the optimal entangled state is the GHZ state $\sqrt{1/2}(|+\rangle^N + |-\rangle^N)$, and that $\mathfrak{J}_N^{(\text{ent})} \rightarrow 3.3N^2T/\gamma$ in the limit of large N and $\omega \rightarrow 0$. Hence, in the limit of large N, T it considerably outperforms all product strategies, yet it is much smaller than $\mathfrak{J}^{(\text{ult})}$, i.e., $\mathfrak{J}_N^{(\text{prod})} \leq \mathfrak{J}_N^{(\text{cd})} \ll \mathfrak{J}_N^{(\text{ent})} \ll \mathfrak{J}^{(\text{ult})}$. This hierarchy of precision limits is shown and summarized in Fig. 3.

Discussion and Conclusions— We studied the precision limits in estimating single-qubit signals under erasure noise across strategy classes of varying complexity. We have shown that for Hamiltonians in the $\sigma_x - \sigma_y$ plane, QEC can introduce a significant metrological gain by correcting the dominant erasure processes. For Hamiltonians in the σ_z direction, the metrological gain is more limited, and the asymptotic optimal protocols involve only spin squeezing. Furthermore, in this case we have shown that product CD protocols outperform optimal passive entangled strategies in the small N regime, highlighting the power of CD strategies. Interesting future research directions include combining CD with entanglement and with optimal coherent control. It would also be interesting to devise more general optimal protocols that rely on erasure conversion and logical spin squeezing.

Acknowledgements— The authors are thankful to Ran Finkelstein, Nelson Darkwah Oppong, Su Direkci, James W. Gardner, and Yanbei Chen for useful discussions. T.G. acknowledges funding from the quantum science and technology early-career grant of the Israeli council for higher education and ISF Grant No. 3302/25. A. R. acknowledges the support of the Israeli Science Foundation, the Israeli Innovation Authority and the Schwartzmann university chair.

Supplemental Material

CONTENTS

I. Ultimate asymptotic precision limits of erasure qubits	1
A. $\mathfrak{J}^{(\text{ult})}$ for erasure qubits with $G \parallel \sigma_z$	2
B. $\mathfrak{J}^{(\text{ult})}$ for erasure qubits with $G \perp \sigma_z$	4
C. $\mathfrak{J}^{(\text{ult})}$ for erasure qubits with general G	6
II. Optimal entangled strategies for $G \parallel \sigma_z$: saturation of $\mathfrak{J}^{(\text{ult})}$ (proof of claim 1)	7
III. Applications to qubits with thermal noise: optimal protocols	10
IV. Optimal quantum error correction protocols for $G \perp \sigma_z$	11
A. Optimal Heisenberg limit protocols for $G \perp \sigma_z$	11
B. Optimal standard quantum limit protocols for $G \perp \sigma_z$	12
V. Single qubit ECQFI bounds and protocols	13
A. $\mathfrak{J}_N^{(\text{prod})}$ for erasure qubits with $G \parallel \sigma_z$	13
B. $\mathfrak{J}_N^{(\text{prod})}$ for erasure qubits with $G \perp \sigma_z$	15
VI. Continuous erasure detection protocols	17
A. $\mathfrak{J}_N^{(\text{cd})}$ for erasure qubits with $G \parallel \sigma_z$	18
B. $\mathfrak{J}_N^{(\text{cd})}$ for erasure qubits with $G \perp \sigma_z$	22

I. ULTIMATE ASYMPTOTIC PRECISION LIMITS OF ERASURE QUBITS

Let us review the sequential ECQFI bounds that were derived in Refs. [23–25]. These bounds are used to calculate $\mathfrak{J}^{(\text{ult})}$ for the various scenarios. We assume a Markovian time evolution given by a Lindblad master equation

$$\frac{d\rho}{dt} = -i[H, \rho] + \sum_{k=1}^r L_k \rho L_k^\dagger - \frac{1}{2} \{L_k^\dagger L_k, \rho\},$$

where H is the Hamiltonian and L_k are the Lindblad jump operators. The Hamiltonian is $H = \omega G$, such that ω is the parameter to be estimated. To find the most general sequential extended-channel QFI (ECQFI) we consider infinitesimal-time evolution Kraus operators given by

$$\mathbf{K} = \begin{pmatrix} \mathbb{1} - i\omega H dt - \frac{1}{2} \sum_k L_k^\dagger L_k dt \\ \sqrt{\gamma_1} L_1 \sqrt{dt} \\ \vdots \\ \sqrt{\gamma_r} L_r \sqrt{dt} \end{pmatrix}.$$

The sequential ECQFI is then given by

$$\mathcal{I} = 4 \min_h \left(\left(\frac{NT}{dt} \right) \|\alpha\| + \left(\frac{NT}{dt} \right)^2 \|\beta\| \left(\|\beta\| + 2\sqrt{\|\alpha\|} \right) \right),$$

where $\alpha = (\mathbf{K} - ih\mathbf{K})^\dagger (\mathbf{K} - ih\mathbf{K})$, $\beta = i\mathbf{K}^\dagger (\mathbf{K} - ih\mathbf{K})$ and h is a Hermitian $(r+1) \times (r+1)$ matrix that acts on the \mathbf{K} vector. It was shown in Refs. [23–25] that, if $G \in \text{span}\{\mathbb{1}, L_i, L_i^\dagger, L_i^\dagger L_j\}_{i,j}$ then there exists h such that $\beta = 0$. The asymptotic bound would then be equal to

$$\mathcal{I} = 4 \left(\frac{NT}{dt} \right) \min_h \|\alpha\|$$

subject to $\beta = 0$.

This expression can be further simplified in the case of infinitesimal channels. We expand α , β , h and \mathbf{K} in powers of \sqrt{dt}

$$\begin{aligned}\alpha &= \alpha^{(0)} + \alpha^{(1)}\sqrt{dt} + \alpha^{(2)}dt + O(dt^{3/2}) \\ \beta &= \beta^{(0)} + \beta^{(1)}\sqrt{dt} + \beta^{(2)}dt + \beta^{(3)}dt^{3/2} + O(dt^2) \\ h &= h^{(0)} + h^{(1)}\sqrt{dt} + h^{(2)}dt + h^{(3)}dt^{3/2} + O(dt^2) \\ \mathbf{K} &= \mathbf{K}^{(0)} + \mathbf{K}^{(1)}\sqrt{dt} + \mathbf{K}^{(2)}dt.\end{aligned}$$

Note that

$$\mathbf{K}^{(0)} = \begin{pmatrix} \mathbb{1} \\ 0 \\ \vdots \\ 0 \end{pmatrix}, \quad \mathbf{K}^{(1)} = \begin{pmatrix} 0 \\ \sqrt{\gamma_1}L_1 \\ \vdots \\ \sqrt{\gamma_r}L_r \end{pmatrix}, \quad \mathbf{K}^{(2)} = \begin{pmatrix} -i\omega H - \frac{1}{2}\sum_j L_j^\dagger L_j \\ 0 \\ \vdots \\ 0 \end{pmatrix}.$$

It can be shown that $\beta = 0$ iff $\beta^{(2)} = G - \sum_{j,k} h_{j,k}^{(0)} L_k^\dagger L_j - \sum_k h_{0,k}^{(1)} (L_k + L_k^\dagger) - h_{0,0}^{(2)} I$ can be set to zero. This is satisfied iff $G \in \text{span}\{\mathbb{1}, L_i, L_i^\dagger, L_i^\dagger L_j\}_{i,j}$. The leading and relevant order of α is $\alpha^{(2)} = (h^{(1)}\mathbf{K}^{(0)} + h^{(0)}\mathbf{K}^{(1)})^\dagger (h^{(1)}\mathbf{K}^{(0)} + h^{(0)}\mathbf{K}^{(1)})$. Therefore given that $G \in \text{span}\{\mathbb{1}, L_i, L_i^\dagger, L_i^\dagger L_j\}_{i,j}$ the asymptotic sequential ECQFI is $4\alpha NT$, with

$$\begin{aligned}\alpha &= \min_h \left(h^{(1)}\mathbf{K}^{(0)} + h^{(0)}\mathbf{K}^{(1)} \right)^\dagger \left(h^{(1)}\mathbf{K}^{(0)} + h^{(0)}\mathbf{K}^{(1)} \right) \\ &\text{subject to } G = \sum_{j,k} h_{j,k}^{(0)} L_k^\dagger L_j + \sum_k h_{0,k}^{(1)} (L_k + L_k^\dagger) + h_{0,0}^{(2)} \mathbb{1}.\end{aligned}\tag{S1}$$

We consider the qubit case where the Hamiltonian $H = \omega G$ acts on a two-level system $\text{span}\{|1\rangle, |2\rangle\}$. Besides of the two level system, there are k erasure states $\{|e_i\rangle\}_{i=1}^k$ to which the qubit decays. We therefore have $2k$ jump operators

$$\left\{ L_{1,j} = \sqrt{\gamma_{1,j}}\sigma_1^{(j)}, L_{2,j} = \sqrt{\gamma_{2,j}}\sigma_2^{(j)} \right\}_{j=1}^k,$$

where $\sigma_1^{(j)} = |e_j\rangle\langle 1|$, $\sigma_2^{(j)} = |e_j\rangle\langle 2|$.

The precision bound depends on the direction of G . Hence, we split the analysis to the following three cases.

A. $\mathfrak{J}^{(\text{ult})}$ for erasure qubits with $G \parallel \sigma_z$

Without loss of generality, $G = \sigma_z$ (for any $G = \alpha\sigma_z$ the QFI is just multiplied by α^2). Let us first consider the case of a single erasure state $|e\rangle$. Note that $\sigma_z = \sigma_1^\dagger\sigma_1 - \sigma_2^\dagger\sigma_2$. The constraint in Eq. S1 is thus

$$\sigma_z = h_{1,1}^{(0)}\gamma_1\sigma_1^\dagger\sigma_1 + h_{2,2}^{(0)}\gamma_2\sigma_2^\dagger\sigma_2 + h_{0,0}^{(2)}\mathbb{1},$$

which implies

$$\begin{aligned}h_{1,1}^{(0)}\gamma_1 + h_{0,0}^{(2)} &= 1 \\ h_{2,2}^{(0)}\gamma_2 + h_{0,0}^{(2)} &= -1.\end{aligned}$$

We can thus express all $h^{(0)}$ terms using $h_{0,0}^{(2)}$. Denoting $\mathfrak{h} := h_{0,0}^{(2)}$ we get

$$\begin{aligned}h^{(0)}\mathbf{K}^{(1)} &= \begin{pmatrix} 0 & & & \\ & \frac{(1-\mathfrak{h})}{\gamma_1} & & \\ & & -\frac{(1+\mathfrak{h})}{\gamma_2} & \\ & & & \end{pmatrix} \begin{pmatrix} 0 \\ \sqrt{\gamma_1}\sigma_1 \\ \sqrt{\gamma_2}\sigma_2 \\ \end{pmatrix} = \begin{pmatrix} 0 \\ \sigma_1 \frac{(1-\mathfrak{h})}{\sqrt{\gamma_1}} \\ -\sigma_2 \frac{(1+\mathfrak{h})}{\sqrt{\gamma_2}} \\ \end{pmatrix} \\ \Rightarrow \alpha^{(2)} &= \sigma_1^\dagger\sigma_1 \frac{(1-\mathfrak{h})^2}{\gamma_1} + \sigma_2^\dagger\sigma_2 \frac{(1+\mathfrak{h})^2}{\gamma_2}.\end{aligned}$$

The optimization problem is thus

$$\min_{\mathfrak{h}} \max \left\{ \frac{(1-\mathfrak{h})^2}{\gamma_1}, \frac{(1+\mathfrak{h})^2}{\gamma_2} \right\}.$$

Observe that the minmax is obtained when $\frac{(1-\mathfrak{h})^2}{\gamma_1} = \frac{(1+\mathfrak{h})^2}{\gamma_2}$. There are two values of \mathfrak{h} for which this equality is attained. The minmax corresponds to the solution at $-1 \leq \mathfrak{h} \leq 1$

$$\mathfrak{h} = \frac{\sqrt{\gamma_2} - \sqrt{\gamma_1}}{\sqrt{\gamma_2} + \sqrt{\gamma_1}} \Rightarrow \min \|\alpha^{(2)}\| = \frac{4}{(\sqrt{\gamma_1} + \sqrt{\gamma_2})^2} \Rightarrow \mathfrak{J}^{(\text{ult})} = \frac{16}{(\sqrt{\gamma_1} + \sqrt{\gamma_2})^2} NT.$$

We now generalize to multiple erasure states, where the jump operators are $\{L_{2j-1} = \sqrt{\gamma_{1,j}}\sigma_{1,j}, L_{2j} = \sqrt{\gamma_{2,j}}\sigma_{2,j}\}_{j=1}^k$. The constraint becomes $\mathbf{K}^{(1)\dagger}h^{(0)}\mathbf{K}^{(1)} = \sigma_z$, i.e.,

$$\sigma_z = \sum_{j=1}^k \left(h_{2j-1,2j-1}^{(0)} \gamma_{1,j} \sigma_{1,j}^\dagger \sigma_{1,j} + h_{2j,2j}^{(0)} \gamma_{2,j} \sigma_{2,j}^\dagger \sigma_{2,j} \right) + h_{0,0}^{(2)} \mathbb{1}$$

and the other terms of h can be set to zero. Denoting $h_{1,j} := h_{2j-1,2j-1}^{(0)}$ and $h_{2,j} := h_{2j,2j}^{(0)}$ we get

$$\begin{aligned} \sum_{j=1}^k h_{1,j} \gamma_{1,j} &= 1 - h_{0,0}^{(2)} \\ \sum_{j=1}^k h_{2,j} \gamma_{2,j} &= -1 - h_{0,0}^{(2)} \end{aligned}$$

which together imply

$$\sum_{j=1}^k (h_{1,j} \gamma_{1,j} - h_{2,j} \gamma_{2,j}) = 2.$$

To compute $\alpha^{(2)}$ we evaluate

$$h^{(0)}\mathbf{K}^{(1)} = \left(\begin{array}{c} h_{1,j} \sqrt{\gamma_{1,j}} \sigma_{1,j} \\ h_{2,j} \sqrt{\gamma_{2,j}} \sigma_{2,j} \end{array} \right)_{j=1}^k \Rightarrow \alpha^{(2)} = \Pi_1 \left(\sum_{j=1}^k h_{1,j}^2 \gamma_{1,j} \right) + \Pi_2 \left(\sum_{j=1}^k h_{2,j}^2 \gamma_{2,j} \right).$$

The optimization problem is

$$\begin{aligned} \min_{\{h_{1,j}, h_{2,j}\}_{j=1}^k} \max & \left\{ \sum_{j=1}^k h_{1,j}^2 \gamma_{1,j}, \sum_{j=1}^k h_{2,j}^2 \gamma_{2,j} \right\} \\ \text{subject to} & \sum_{j=1}^k (h_{1,j} \gamma_{1,j} - h_{2,j} \gamma_{2,j}) = 2. \end{aligned}$$

Note that for smooth and convex functions the minimizer of $\max(f_1(\mathbf{x}), f_2(\mathbf{x}))$ lies among

$$\min f_1(\mathbf{x}), \min f_2(\mathbf{x}), \text{ or } \min_{x: f_1(\mathbf{x})=f_2(\mathbf{x})} f_2(\mathbf{x}).$$

We first consider the case when both terms are equal. Let λ, μ be Lagrange multipliers, and define the Lagrangian

$$\mathfrak{L} = \sum_{j=1}^k h_{1,j}^2 \gamma_{1,j} + \lambda \left(\sum_{j=1}^k (h_{1,j} \gamma_{1,j} + h_{2,j} \gamma_{2,j}) - 2 \right) + \mu \sum_{j=1}^k (h_{2,j}^2 \gamma_{2,j} - h_{1,j}^2 \gamma_{1,j}).$$

Setting gradients to zero

$$\begin{aligned} \frac{\nabla \mathcal{L}}{h_{1,j}} = 0 &\Rightarrow 2h_{1,j} + \lambda - 2\mu h_{1,j} = 0 \\ \frac{\nabla \mathcal{L}}{h_{2,j}} = 0 &\Rightarrow \lambda + 2\mu h_{1,j} = 0. \end{aligned}$$

Notably, all $h_{1,j}$ are equal, and likewise all $h_{2,j}$. This holds not only at the intersection of the two terms, but also when minimizing each term individually, as can be seen by repeating the Lagrangian process for each. Using this, define $\mathfrak{h} := 1 - h_{1,j} \sum_{j=1}^k \gamma_{1,j}$, and using our constraint we express all terms using \mathfrak{h}

$$\min_{\{h\}} \|\alpha^{(2)}\| = \min_{\{h_{1,j}, h_{2,j}\}_{j=1}^k} \max \left\{ \frac{(\mathfrak{h}-1)^2}{\sum_{j=1}^k \gamma_{1,j}}, \frac{(\mathfrak{h}+1)^2}{\sum_{j=1}^k \gamma_{2,j}} \right\} \Rightarrow \mathcal{J}^{(\text{ult})} = \frac{16}{(\sqrt{\Gamma_1} + \sqrt{\Gamma_2})^2} NT.$$

where $\Gamma_i = \sum_{j=1}^k \gamma_{i,j}$, as defined also in the main text.

B. $\mathcal{J}^{(\text{ult})}$ for erasure qubits with $G \perp \sigma_z$

Without loss of generality we can take $G = \sigma_x$. Let us first consider the case of a single erasure state $|e\rangle$. Note that $\sigma_x = \sigma_1^\dagger \sigma_2 + \text{h.c.}$. Hence the constraint of Eq. S1 is

$$\sigma_x = h_{1,2}^{(0)} \sqrt{\gamma_2 \gamma_1} \sigma_1^\dagger \sigma_2 + h_{2,1}^{(0)} \sqrt{\gamma_2 \gamma_1} \sigma_2^\dagger \sigma_1,$$

which implies $h_{1,2}^{(0)} = 1/\sqrt{\gamma_2 \gamma_1}$. Therefore,

$$h^{(0)} \mathbf{K}^{(1)} = \left(\begin{array}{c} \frac{\sqrt{\gamma_1}}{\sqrt{\gamma_1 \gamma_2}} \sigma_1 \\ \frac{\sqrt{\gamma_2}}{\sqrt{\gamma_2 \gamma_1}} \sigma_2 \end{array} \right) \Rightarrow \alpha^{(2)} = (h^{(0)} \mathbf{K}^{(1)})^\dagger (h^{(0)} \mathbf{K}^{(1)}) = \frac{1}{\gamma_2} \sigma_1^\dagger \sigma_1 + \frac{1}{\gamma_1} \sigma_2^\dagger \sigma_2.$$

We therefore get that

$$\min_h \|\alpha^{(2)}\| = \frac{1}{\min\{\gamma_1, \gamma_2\}} \Rightarrow \mathcal{J}^{(\text{ult})} = \frac{4}{\min\{\gamma_1, \gamma_2\}} NT. \quad (\text{S2})$$

Let us now consider the case of several erasure states, i.e., we have the following jump operators: $\{L_{2j-1} = \sqrt{\gamma_{1,j}} \sigma_{1,j}, L_{2j} = \sqrt{\gamma_{2,j}} \sigma_{2,j}\}_{j=1}^k$. The constraint of Eq. S1 is thus $\mathbf{K}^{(1)\dagger} h^{(0)} \mathbf{K}^{(1)} = \sigma_x$, i.e.,

$$\sigma_x = \sum_{j=1}^k h_{2j-1,2j}^{(0)} \sqrt{\gamma_{1,j} \gamma_{2,j}} \sigma_{1,j}^\dagger \sigma_{2,j} + h_{2j,2j-1}^{(0)} \sqrt{\gamma_{1,j} \gamma_{2,j}} \sigma_{2,j}^\dagger \sigma_{1,j} = \sum_{j=1}^k h_{2j-1,2j}^{(0)} \sqrt{\gamma_{1,j} \gamma_{2,j}} \sigma_x.$$

Denoting $h_j := h_{2j-1,2j}^{(0)}$ we get that the constraint is

$$\sum_{j=1}^k h_j \sqrt{\gamma_{1,j} \gamma_{2,j}} = 1.$$

To derive the objective note that

$$h^{(0)} \mathbf{K}^{(1)} = \left(\begin{array}{c} h_j \sqrt{\gamma_{1,j}} \sigma_{1,j} \\ h_j \sqrt{\gamma_{2,j}} \sigma_{2,j} \end{array} \right)_{j=1}^k \Rightarrow \alpha^{(2)} = \Pi_1 \left(\sum_{j=1}^k h_j^2 \gamma_{1,j} \right) + \Pi_2 \left(\sum_{j=1}^k h_j^2 \gamma_{2,j} \right).$$

The optimization is thus

$$\begin{aligned} \min_{\{h_j\}_j} \|\alpha^{(2)}\| &= \min_{\{h_j\}_j} \max \left\{ \sum_{j=1}^k h_j^2 \gamma_{2,j}, \sum_{j=1}^k h_j^2 \gamma_{1,j} \right\} \\ \text{subject to} & \sum_{j=1}^k h_j \sqrt{\gamma_{1,j} \gamma_{2,j}} = 1. \end{aligned} \quad (\text{S3})$$

This problem can be solved in general using an SDP. Defining $A = \mathbf{m}\mathbb{1} - \text{diag}\left(\sum_{j=1}^k h_j^2 \gamma_{2,j}, \sum_{j=1}^k h_j^2 \gamma_{1,j}\right)$, the SDP reads

$$\begin{aligned} & \min \mathbf{m} \\ & \text{subject to } A \geq 0 \\ & \sum_{j=1}^k h_j \sqrt{\gamma_{1,j} \gamma_{2,j}} = 1. \end{aligned}$$

The solution then corresponds to $\min_{\{h_j\}_j} \|\alpha^{(2)}\|$. By solving this problem numerically for different cases it can be observed that $\mathfrak{J}^{(\text{ult})}$ in general lies within this range

$$\left[2 \sum_{j=1}^k \min(\gamma_{1,j}, \gamma_{2,j}) \right]^{-1} \leq \min_{\{h_j\}_j} \|\alpha^{(2)}\| \leq \left[\sum_{j=1}^k \min(\gamma_{1,j}, \gamma_{2,j}) \right]^{-1}. \quad (\text{S4})$$

Let us prove this observation.

Proof: We first prove the inequality: $\min_{\{h_j\}_j} \|\alpha^{(2)}\| \leq \left[\sum_{j=1}^k \min(\gamma_{1,j}, \gamma_{2,j}) \right]^{-1}$. Note that

$$\min_{\{h_j\}_j} \left[\max \left(\sum_{j=1}^k h_j^2 \gamma_{1,j}, \sum_{j=1}^k h_j^2 \gamma_{2,j} \right) \right] \leq \min_{\{h_j\}_j} \left[\sum_{j=1}^k h_j^2 \max(\gamma_{1,j}, \gamma_{2,j}) \right] \leq \left[\sum_{j=1}^k \min(\gamma_{1,j}, \gamma_{2,j}) \right]^{-1},$$

where the last inequality is obtained by choosing $h_j = \frac{1}{\sum_m \min(\gamma_{1,m}, \gamma_{2,m})} \sqrt{\frac{\min(\gamma_{1,j}, \gamma_{2,j})}{\max(\gamma_{1,j}, \gamma_{2,j})}}$, which satisfies the constraint in Eq. S3.

The inequality $\left[2 \sum_{j=1}^k \min(\gamma_{1,j}, \gamma_{2,j}) \right]^{-1} \leq \min_{\{h_j\}_j} \|\alpha^{(2)}\|$ is proven by constructing a QEC protocol that achieves this QFI. Consider the code space spanned by $\{|0_L\rangle = |+\rangle|0\rangle_a, |1_L\rangle = |-\rangle|1\rangle_a\}$, with a recovery operation

$$\begin{aligned} & |e_j\rangle|0\rangle_a \rightarrow |+\rangle|0\rangle_a, |e_j\rangle|1\rangle_a \rightarrow (-1)^{f_j} |-\rangle|1\rangle_a \\ & \text{where } f_j = \begin{cases} 1 & \gamma_{1,j} \geq \gamma_{2,j} \\ 2 & \text{otherwise.} \end{cases} \end{aligned}$$

Performing QEC continuously leads to the following logical dephasing dynamics

$$\frac{d\rho}{dt} = -i\omega [\sigma_z^L, \rho] + \gamma_{\text{eff}} (\sigma_z^L \rho \sigma_z^L - \rho)$$

with $\gamma_{\text{eff}} = \frac{1}{2} \sum_j \min\{\gamma_{1,j}, \gamma_{2,j}\}$. We refer to Appendix IV and to Refs. [28] for a derivation of this effective dynamics. It was shown that, under this dynamics, an optimal logical spin squeezed state achieves a QFI of $I = \frac{NT}{\gamma_{\text{eff}}}$ [28]. Hence, we obtain a QFI of $I = \frac{NT}{\gamma_{\text{eff}}} = \frac{NT}{\frac{1}{2} \sum_j \min\{\gamma_{1,j}, \gamma_{2,j}\}}$, and thus $\|\alpha^{(2)}\| \geq \left[2 \sum_j \min\{\gamma_{1,j}, \gamma_{2,j}\} \right]^{-1}$.

We remark that the upper bound of $\frac{4T}{\sum_{j=1}^k \min(\gamma_{1,j}, \gamma_{2,j})}$ is saturable in the case where the decay from one of the states is dominant, i.e., where $\forall j \gamma_{1,j} \leq \gamma_{2,j}$ and equivalently $\forall j \gamma_{1,j} \geq \gamma_{2,j}$. This can be seen explicitly from the optimization problem of Eq. S3: assuming wlog that $\gamma_{1,j} \leq \gamma_{2,j}$ the minimization becomes $\min_{\mathbf{h}} \sum_{j=1}^k h_j^2 \gamma_{2,j}$ subject to $\sum_{j=1}^k h_j \sqrt{\gamma_{2,j} \gamma_{1,j}} = 1$. Using Cauchy-Schwartz inequality

$$\left(\sum_{j=1}^k h_j \sqrt{\gamma_{2,j} \gamma_{1,j}} \right)^2 \leq \left(\sum_{j=1}^k h_j^2 \gamma_{2,j} \right) \left(\sum_{j=1}^k \gamma_{1,j} \right)$$

we obtain that the minimum is indeed $\frac{1}{\sum_{j=1}^k \gamma_{1,j}}$. This also implies that for $\gamma_{1,j} = \gamma_{2,j} = \gamma_j$ the ECQFI is $\frac{4T}{\sum_{j=1}^k \gamma_j}$, which is the same as in the case of $G \parallel \sigma_z$, since given identical decays from $|1\rangle$ and $|2\rangle$ there is no difference between the different Pauli operators.

We can further illustrate the bounds by considering the special case illustrated in Fig. S1 (a): two erasure states with decay rates of $\gamma_{\min} := \gamma_{1,1} = \gamma_{2,2} < \gamma_{\max} := \gamma_{1,2} = \gamma_{2,1}$. The dominant decay to $|e_1\rangle$ is from $|2\rangle$ while the dominant decay to $|e_2\rangle$ is from $|1\rangle$. The resulting sequential ECQFI bounds are illustrated in Fig. S1 (b). It can be seen that as $\gamma_{\max} \rightarrow \gamma_{\min}$ the bound converges to $4 \frac{T}{\sum_j \min\{\gamma_{1,j}, \gamma_{2,j}\}} = \frac{2T}{\gamma_{\min}}$. While in the limit of $\gamma_{\max} \gg \gamma_{\min}$ the bound converges to $2 \frac{T}{\sum_j \min\{\gamma_{1,j}, \gamma_{2,j}\}} = \frac{T}{\gamma_{\min}}$.

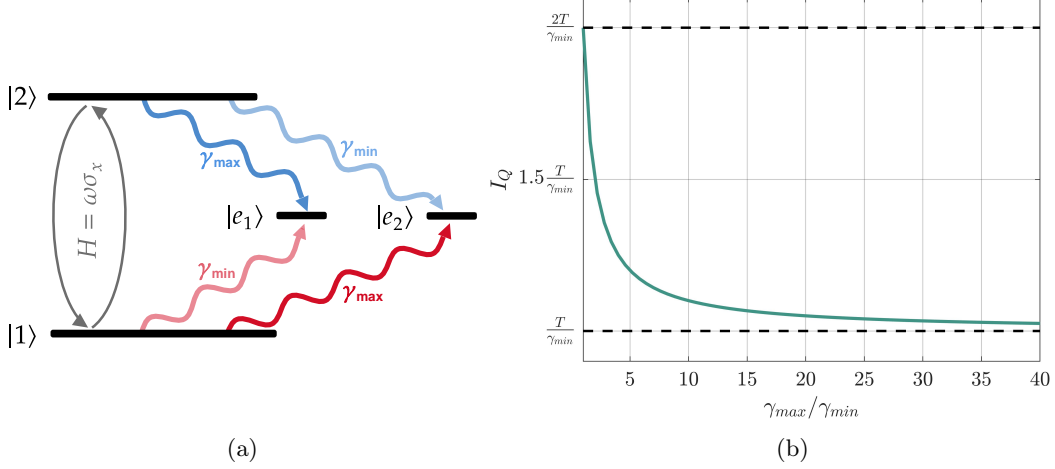


Figure S1: (a) Sketch of the erasure configuration: $G = \sigma_x$ with two erasure states such that $\gamma_{\min} := \gamma_{1,1} = \gamma_{2,2} < \gamma_{\max} := \gamma_{1,2} = \gamma_{2,1}$. (b) $\mathcal{J}^{(\text{ult})}$ given this erasure configuration, it can be seen that the precision limits lie between the lower and upper bounds of Eq. S4 depending on $\gamma_{\max}/\gamma_{\min}$.

C. $\mathcal{J}^{(\text{ult})}$ for erasure qubits with general G

Without loss of generality we can take $G = \cos\theta\sigma_z + \sin\theta\sigma_x$ with $\theta \in [0, \frac{\pi}{2}]$. Our analysis of this case assumes a single erasure state $|e\rangle$. The constraint in Eq. S1 is thus

$$\cos\theta\sigma_z + \sin\theta\sigma_x = h_{1,1}^{(0)}\gamma_1\sigma_1^\dagger\sigma_1 + h_{2,2}^{(0)}\gamma_2\sigma_2^\dagger\sigma_2 + h_{1,2}^{(0)}\sqrt{\gamma_2\gamma_1}\sigma_1^\dagger\sigma_0 + h_{2,1}^{(0)}\sqrt{\gamma_2\gamma_1}\sigma_2^\dagger\sigma_1 + h_{0,0}^{(2)}\mathbb{1}$$

which implies

$$\begin{aligned} h_{1,1}^{(0)}\gamma_1 + h_{0,0}^{(2)} &= \cos\theta \\ h_{2,2}^{(0)}\gamma_2 + h_{0,0}^{(2)} &= -\cos\theta \\ h_{1,2}^{(0)} &= h_{2,1}^{(0)} = \sin\theta/\sqrt{\gamma_1\gamma_2}. \end{aligned}$$

We can thus express all $h^{(0)}$ terms using $h_{0,0}^{(2)}$. Denoting $\mathfrak{h} := h_{0,0}^{(2)}$ we get

$$\begin{aligned} h^{(0)}\mathbf{K}^{(1)} &= \begin{pmatrix} 0 & \frac{(\cos\theta - \mathfrak{h})}{\gamma_1} & \frac{\sin\theta}{\sqrt{\gamma_1\gamma_1}} \\ \frac{\sin\theta}{\sqrt{\gamma_1\gamma_1}} & -\frac{(\cos\theta + \mathfrak{h})}{\gamma_2} & 0 \end{pmatrix} \begin{pmatrix} 0 \\ \sqrt{\gamma_1}\sigma_1 \\ \sqrt{\gamma_2}\sigma_2 \end{pmatrix} = \begin{pmatrix} 0 \\ \frac{(\cos\theta - \mathfrak{h})\sigma_1 + \sin\theta\sigma_2}{\sqrt{\gamma_1}} \\ -\frac{(\cos\theta + \mathfrak{h})\sigma_2 + \sin\theta\sigma_1}{\sqrt{\gamma_2}} \end{pmatrix} \\ \Rightarrow \alpha^{(2)} &= \Pi_1 \left(\frac{(\cos\theta - \mathfrak{h})^2}{\gamma_1} + \frac{\sin^2\theta}{\gamma_2} \right) + \Pi_2 \left(\frac{(\cos\theta + \mathfrak{h})^2}{\gamma_2} + \frac{\sin^2\theta}{\gamma_1} \right) + \sigma_x \left(\frac{\sin\theta(\cos\theta - \mathfrak{h})}{\gamma_1} - \frac{\sin\theta(\cos\theta + \mathfrak{h})}{\gamma_2} \right), \end{aligned}$$

where $\Pi_j = |j\rangle\langle j|$. The eigenvalues of this $\alpha^{(2)}$ are

$$\lambda_{\pm} = \frac{1}{2\gamma_1\gamma_2} \left[(1 + \mathfrak{h}^2)(\gamma_1 + \gamma_2) + 2\mathfrak{h}\cos\theta(\gamma_1 - \gamma_2) \pm \sqrt{-4(-1 + \mathfrak{h}^2)^2\gamma_1\gamma_2 + [(1 + \mathfrak{h}^2)(\gamma_1 + \gamma_2) + 2\mathfrak{h}\cos\theta(\gamma_1 - \gamma_2)]^2} \right]$$

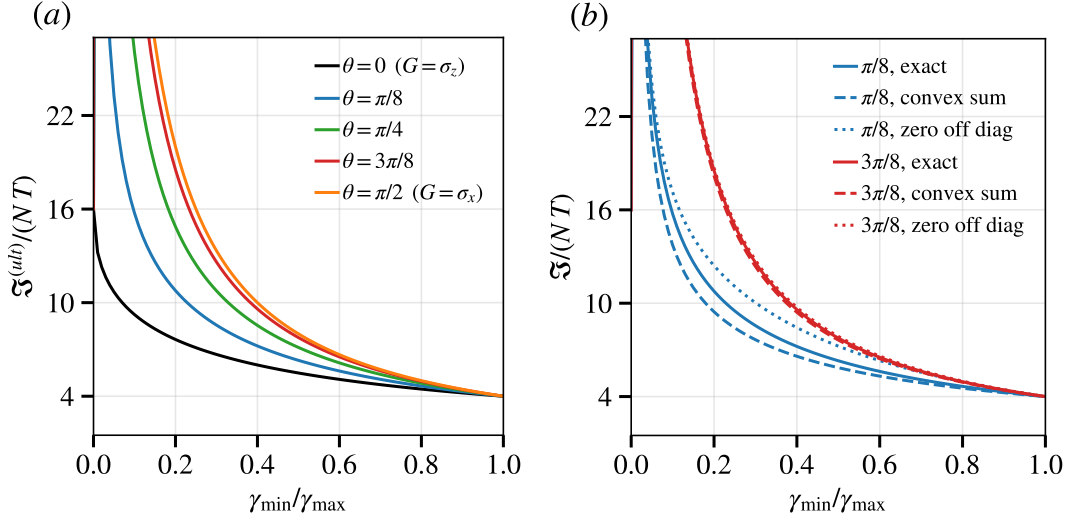


Figure S2: $\mathfrak{J}^{(\text{ult})}$ for $G = \cos \theta \sigma_z + \sin \theta \sigma_x$ as a function of $\gamma_{\min}/\gamma_{\max}$. (a) Exact bounds for several values of θ . (b) For $\theta = \pi/8$ (blue) and $3\pi/8$ (red), comparison of the exact bound (solid) with the convex-sum lower bound of Eq. S6 (dashed), and with the analytic upper bound of Eq. S5 (dotted).

We thus obtain

$$\min_h \|\alpha^{(2)}\| = \min_h \max \{\lambda_+, \lambda_-\} = \min_h \lambda_+ \Rightarrow \boxed{\mathfrak{J}^{(\text{ult})} = 4NT \min_h \lambda_+}.$$

We do not have a closed-form solution to this minimization problem and solve it only numerically. The results are plotted in Fig. S2. To derive an analytic upper bound, we set the off diagonal terms of $\alpha^{(2)}$ to zero. This occurs when $h = -\frac{\gamma_1 - \gamma_2}{\gamma_1 + \gamma_2} \cos \theta$ which yields

$$\mathcal{I}_{\text{zero}} = 4T \left(\frac{4\gamma_1}{(\gamma_1 + \gamma_2)^2} \cos^2 \theta + \frac{\sin^2 \theta}{\gamma_2} \right). \quad (\text{S5})$$

This upper bound is shown in dotted lines in Fig. S2. For comparison, we also include (in dashed lines) the convex sum lower bound:

$$\mathcal{I}_{\text{convex}} = \cos^2 \theta \mathfrak{J}_{\sigma_z}^{(\text{ult})} + \sin^2 \theta \mathfrak{J}_{\sigma_x}^{(\text{ult})}, \quad (\text{S6})$$

where $\mathfrak{J}_{\sigma_m}^{(\text{ult})}$ corresponds to the ultimate limit given $G = \sigma_m$. We observe that these lower and upper bounds are more accurate as θ approaches $\pi/2$ and when $\gamma_{\min}/\gamma_{\max}$ is close to 0 or 1.

II. OPTIMAL ENTANGLED STRATEGIES FOR $G \parallel \sigma_z$: SATURATION OF $\mathfrak{J}^{(\text{ult})}$ (PROOF OF CLAIM 1)

In this section we prove Claim 1 of the main text, i.e., we show that $\mathfrak{J}^{(\text{ult})}$ is saturated in the limit of $N \rightarrow \infty$ for $G = \sigma_z$ with the strategy class (ii) (entangled states) by using an optimal ancilla-free spin squeezed state. Considering N qubits, let us define the total spin operators: $J_m := \frac{1}{2} \sum_{i=1}^N \sigma_m^{(i)}$, where $m \in \{x, y, z\}$. We take as an initial state the following spin squeezed state [52]

$$|\psi_{\phi, \chi}^{\text{sq}}\rangle = e^{-i\phi J_y} e^{i\chi(J_z J_y + J_y J_z)} e^{i\frac{\pi}{2} J_y} |1\rangle^{\otimes N}. \quad (\text{S1})$$

The first pulse $e^{i\frac{\pi}{2} J_y}$ maps $|1\rangle^{\otimes N}$ into the spin coherent state $|+\rangle^{\otimes N}$. The qubits then evolve under the two-axis twisting Hamiltonian $\chi(J_z J_y + J_y J_z)$ which squeezes $\text{var}(J_y)$. The final pulse $e^{-i\phi J_y}$ is a rotation along the Y-axis,

after which $\langle J_x \rangle \approx \frac{N}{2} \cos(\phi)$, $\langle J_z \rangle \approx \frac{N}{2} \sin(\phi)$. At large N , the QFI of these states can be approximated (and lower bounded) by the error propagation formula [63, 67]

$$I \geq \frac{(\partial_\omega \langle J_x \rangle_t)^2}{\text{var}(J_x)_t}. \quad (\text{S2})$$

It therefore suffices to show that the error propagation expression converges to $\mathfrak{J}^{(\text{ult})}$. To calculate this bound we need to find the time evolution of $\langle J_x \rangle$, $\text{var}(J_x)$ given our erasure channel. Defining $\eta_i = e^{-\Gamma_i t}$ (for $i = 1, 2$) we obtain

$$\begin{aligned} \langle J_x \rangle_t &= \sqrt{\eta_1 \eta_2} (\cos(\varphi) \langle J_x \rangle_0 - \sin(\varphi) \langle J_y \rangle_0), \\ \partial_\omega \langle J_x \rangle_t &= -\sqrt{\eta_1 \eta_2} 2t (\sin(\varphi) \langle J_x \rangle_0 + \cos(\varphi) \langle J_y \rangle_0), \end{aligned} \quad (\text{S3})$$

where $\varphi = 2\omega t$. $\text{var}(J_x)$ evolves as

$$\begin{aligned} \text{var}(J_x)_t &= \left(\frac{\eta_1(1-\eta_2) + \eta_2(1-\eta_1)}{8} \right) N \\ &+ \frac{1}{4} [\eta_1(1-\eta_2) - \eta_2(1-\eta_1)] \langle J_z \rangle_0 \\ &+ \eta_1 \eta_2 [\cos^2(\varphi) \text{var}(J_x)_0 + \sin^2(\varphi) \text{var}(J_y)_0 - 2 \sin(\varphi) \cos(\varphi) \text{cov}(J_x, J_y)_0]. \end{aligned} \quad (\text{S4})$$

From Eqs. S3, S4 we observe that the maximal signal and minimal noise are obtained at $\varphi = \pi/2$. Since φ is tunable (we can vary the measurement basis in the $J_x - J_y$ plane), we can assume this value of φ . Inserting Eqs. S3, S4 in the error propagation formula (Eq. S2) yields

$$\frac{\eta_1 \eta_2 \langle J_x \rangle_0^2}{\left(\frac{\eta_1(1-\eta_2) + \eta_2(1-\eta_1)}{8} \right) N + \frac{1}{4} [\eta_1(1-\eta_2) - \eta_2(1-\eta_1)] \langle J_z \rangle_0 + \eta_1 \eta_2 \text{var}(J_y)_0} 4t^2. \quad (\text{S5})$$

In the limit of large N , we can neglect the squeezed $\text{var}(J_y)_0$ (since $\text{var}(J_y)_0/N \rightarrow 0$) and insert $\langle J_x \rangle \approx \frac{N}{2} \cos(\phi)$, $\langle J_z \rangle \approx \frac{N}{2} \sin(\phi)$, to get

$$\frac{\eta_1 \eta_2 \cos^2(\phi) / 4}{\left(\frac{\eta_1(1-\eta_2) + \eta_2(1-\eta_1)}{8} \right) + \frac{1}{8} [\eta_1(1-\eta_2) - \eta_2(1-\eta_1)] \sin(\phi)} 4Nt^2 \quad (\text{S6})$$

$$= \frac{\cos^2(\phi)^2}{(l_1 + l_2) + (l_2 - l_1) \sin(\phi)} 8Nt^2, \quad (\text{S7})$$

where $l_1 = \frac{1-\eta_1}{\eta_1}$, $l_2 = \frac{1-\eta_2}{\eta_2}$. We now need to minimize over both ϕ, t , this optimization can be performed separately: we first find optimal ϕ , and then optimal t . The maximization over ϕ is equivalent to

$$\min_{\phi} \frac{l_1}{1 + \sin(\phi)} + \frac{l_2}{1 - \sin(\phi)}. \quad (\text{S8})$$

The optimal ϕ satisfies $\sin(\phi_{\text{opt}}) = \frac{\sqrt{l_1} - \sqrt{l_2}}{\sqrt{l_2} + \sqrt{l_1}} = \frac{\sqrt{\eta_2(1-\eta_1)} - \sqrt{\eta_1(1-\eta_2)}}{\sqrt{\eta_2(1-\eta_1)} + \sqrt{\eta_1(1-\eta_2)}}$, and the minimum is $\frac{(\sqrt{l_1} + \sqrt{l_2})^2}{2}$. The error propagation expression then reduces to

$$\frac{2}{(\sqrt{l_1} + \sqrt{l_2})^2} 8Nt^2 = \frac{2\eta_1 \eta_2}{(\sqrt{1-\eta_2} + \sqrt{1-\eta_1})^2} 8Nt^2 = \frac{e^{-(\Gamma_1 + \Gamma_2)t}}{(\sqrt{1 - e^{-\Gamma_1 t}} + \sqrt{1 - e^{-\Gamma_2 t}})^2} 16Nt^2. \quad (\text{S9})$$

The optimization of the rate over t is thus

$$\max_t \frac{e^{-(\Gamma_1 + \Gamma_2)t}}{(\sqrt{1 - e^{-\Gamma_1 t}} + \sqrt{1 - e^{-\Gamma_2 t}})^2} 16Nt = \boxed{\frac{16}{(\sqrt{\Gamma_1} + \sqrt{\Gamma_2})^2} N}. \quad (\text{S10})$$

We thus obtained $\mathfrak{J}^{(\text{ult})}/T$, and this establishes the convergence of spin squeezed states to the ultimate asymptotic precision bound and proves Claim 1.

The analysis above corresponds to the asymptotic behavior of the entangled strategy. We further evaluated $\mathfrak{J}_N^{(\text{ent})}$ for finite N . The performance of optimal entangled states and optimal spin squeezed states is shown in Fig. S3. We calculated the optimal entangled strategy for up to $N = 10$ numerically using ECQFI and iterative see-saw (ISS) method [32, 55, 68]. For larger N , ISS becomes intractable and we use a tensor-network based approach to evaluate $\mathfrak{J}_N^{(\text{ent})}$, the ISS-tnet of QMETRO++ package [32]. As shown in Fig. S3, the ISS-tnet results are not exact, yet they provide a good approximation of $\mathfrak{J}_N^{(\text{ent})}$. The performance of optimal spin squeezed states was obtained by optimizing the QFI rate over the squeezing rate χ , the rotation angle ϕ , (see Eq. S1) and the measurement time t . It can be observed that the optimal spin squeezed state strategy yields QFI that matches the values obtained with ISS-tnet for large N . This provides a numerical evidence for the optimality of spin squeezed states already for $N \geq 30$. The Husimi function of the optimal entangled states and optimal spin squeezed states for different N, Γ_1, Γ_2 is illustrated in Fig. S4. We can observe that for $N = 10$ for Γ_{\min} close to Γ_{\max} the optimal entangled state is a spin squeezed state, while in the asymmetric case of $\Gamma_{\min} \ll \Gamma_{\max}$ the optimal state is not a spin squeezed state. It will become a spin squeezed only for larger N .

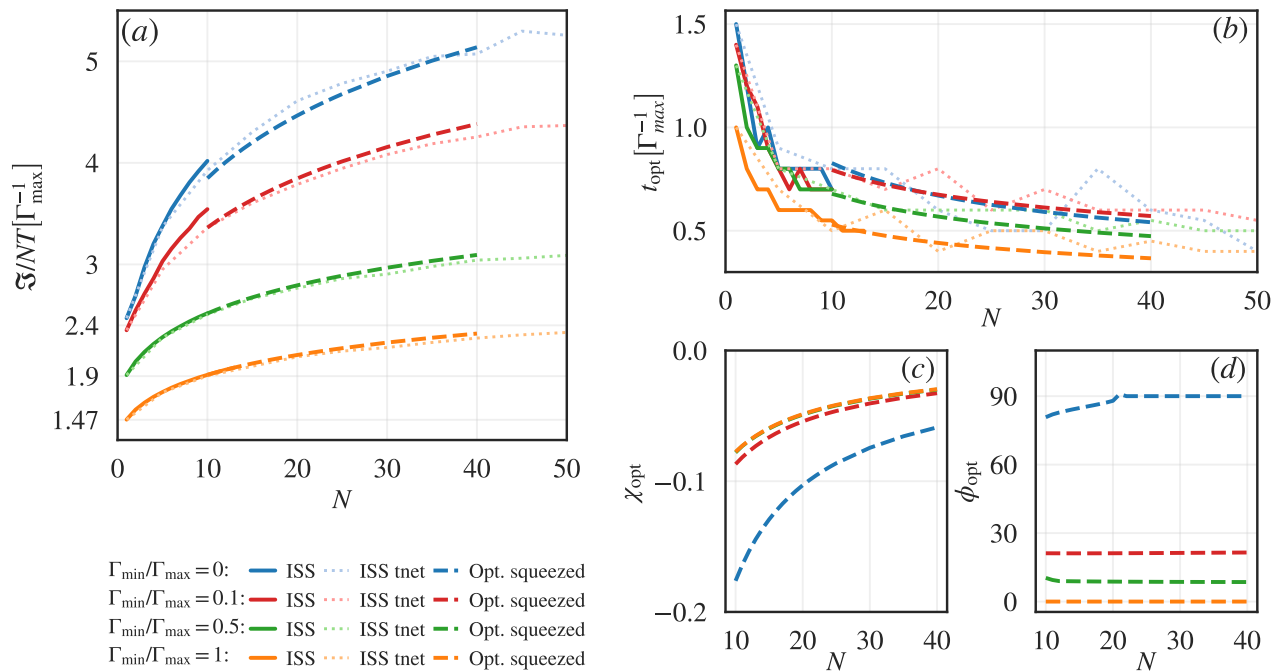


Figure S3: Optimal entangled strategies and spin squeezed state strategies given $G = \sigma_z$ and for different N, Γ_1, Γ_2 . (a) The QFI with optimal entangled state strategies and optimal spin squeezed state strategies as a function of N .

The solid lines correspond to exact optimal entangled states strategies, calculated using ISS. The dotted lines correspond to the optimal entangled QFI obtained with ISS-tnet numerical calculation. The ISS-tnet values provide an approximation of $\mathfrak{J}_N^{(\text{ent})}$. The dashed lines correspond to the QFI with the optimal spin-squeezed states. (b) Optimal measurement time as a function of N . (c) Optimal spin squeezing rate χ as a function of N . (d) Optimal rotation angle of the spin squeezed state, ϕ , as a function of N .

The channel QFI and ISS calculations were performed using an analogy between our N erasure qubits and a lossy two bosonic modes interferometer. This analogy was previously studied in Refs. [21, 63]. Instead of working in the 2^N dimensional Hilbert space of N qubits, the problem can be reduced to the Hilbert space of two bosonic modes with a total number of photons $\leq N$, which is $(N+1)(N+2)/2$ -dimensional. Note that the input state and the unitary dynamics are restricted to the N -qubits symmetric subspace, which is $N+1$ dimensional. The erasure noise takes us out of this subspace, since the state after an erasure decay is not symmetric anymore. However, since there is no information in the erasure state we can trace out the qubits that decayed. The state after tracing out an erased qubit corresponds to a symmetric $(N-1)$ -qubits state. This implies that the relevant Hilbert space corresponds to

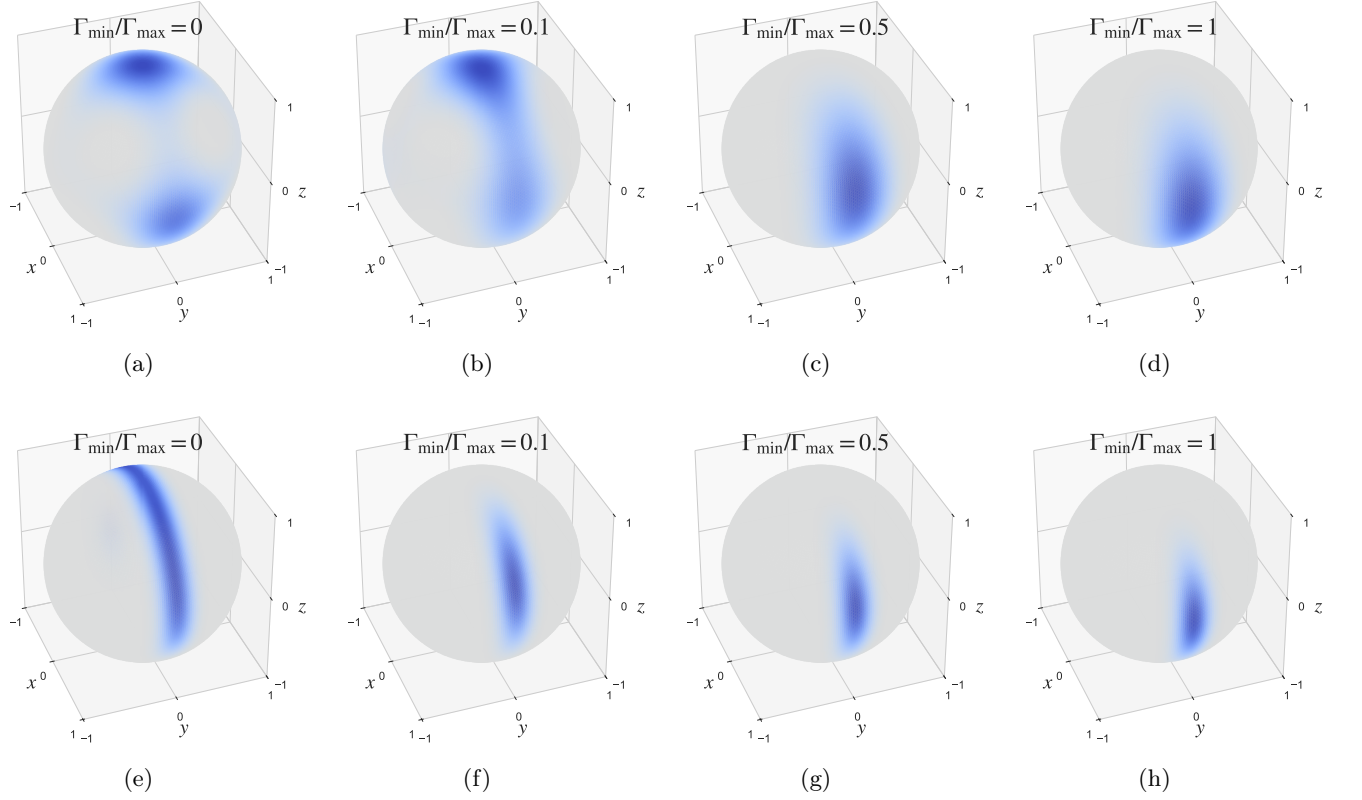


Figure S4: (a-d) Optimal entangled states for $N = 10$ obtained via ISS calculation, and (e-f) optimized spin squeezed states for $N = 40$, shown for different $\Gamma_{\min}/\Gamma_{\max}$ ratios.

$\bigoplus_{k=0}^N \mathcal{H}_{\text{symm},k}$, where $\mathcal{H}_{\text{symm},k}$ is the symmetric subspace of k qubits. Furthermore the dynamics is isomorphic to the dynamics of two bosonic modes in a lossy interferometer. The space $\mathcal{H}_{\text{symm},k}$ is isomorphic to the space of k photons in two modes. The rest of the isomorphism is given as follows:

$$\omega J_z \leftrightarrow \omega (a_1^\dagger a_1 - a_2^\dagger a_2), \quad \Gamma_k \sum_{j=1}^N D[\sigma_k^{(j)}] \leftrightarrow \Gamma_k D[a_k], \quad (\text{S11})$$

and the number of photons in bosonic mode 1 (2) corresponds to the number of qubits in state $|1\rangle$ ($|2\rangle$).

Hence the N qubits dynamics can be reduced to the following two-bosonic modes evolution:

$$\frac{d\rho}{dt} = -i\omega [a_1^\dagger a_1 - a_2^\dagger a_2, \rho] + \sum_{i=1,2} \Gamma_i \left(a_i \rho a_i^\dagger - \frac{1}{2} \{ \rho, a_i^\dagger a_i \} \right). \quad (\text{S12})$$

This simplified dynamics allows us to perform ECQFI calculations up to $N = 7$ and ISS calculations up to $N = 10$. The results are shown in Figs. S3 and S4.

III. APPLICATIONS TO QUBITS WITH THERMAL NOISE: OPTIMAL PROTOCOLS

We derive in this Appendix an erasure conversion scheme for achieving \mathcal{J}^{ult} in the $N \rightarrow \infty$ limit for qubits with thermal noise and $G = \sigma_z$. This scheme uses erasure conversion and then applies the same optimal spin squeezing of Appendix II on the effective erasure qubits. We consider qubits evolving under the following standard thermal Lindblad master equation

$$\frac{d\rho}{dt} = -i[\omega\sigma_z, \rho] + \Gamma_2 D[\sigma_-] \rho + \Gamma_1 D[\sigma_+] \rho, \quad (\text{S1})$$

where ω is the parameter to be estimated, and $\sigma_- = |1\rangle\langle 2|$, $\sigma_+ = \sigma_-^\dagger$. The case of $\Gamma_2 = 0$ corresponds to amplitude damping noise. $\mathcal{J}^{(\text{ult})}$ of this problem is the same as with erasure decay rates of Γ_1, Γ_2 , i.e., Eq. 2 in the main text. Let us define the two-qubits code space: $\{|0\rangle_L = |11\rangle, |1\rangle_L = |22\rangle\}$. This logical code-space is the effective erasure qubit. The jump operators $\sigma_{-,+}^{(j)}$ map this code space into the orthogonal erasure subspace spanned by $\{|12\rangle, |21\rangle\}$. Consider a protocol in which a continuous parity measurement of the physical qubits is performed, indicating whether they are in the code-space or decayed to the erasure subspace. Whenever an erasure was detected we simply discard the relevant two physical qubits. This protocol leads to the following effective erasure dynamics of each logical qubit

$$\frac{d\rho}{dt} = -i [2\omega\sigma_z^L, \rho] + 2\Gamma_1 D[\sigma_1] \rho + 2\Gamma_2 D[\sigma_2] \rho, \quad (\text{S2})$$

where $\sigma_j = |e\rangle\langle j|$ are the erasure jump operators, and $\sigma_z^L = |1_L\rangle\langle 1_L| - |0_L\rangle\langle 0_L|$. We thus obtained a logical dynamics of $L_1 = \sqrt{2}\Gamma_1\sigma_1, L_2 = \sqrt{2}\Gamma_2\sigma_2, H = 2\omega\sigma_z^L$, with $N/2$ logical qubits. The corresponding $\mathcal{J}^{(\text{ult})}$ is the same as the original thermal noise problem: $\mathcal{J}^{(\text{ult})} = 4\frac{16T}{2(\Gamma_1+\Gamma_2)}\frac{N}{2} = \frac{16NT}{\Gamma_1+\Gamma_2}$. Since optimal spin squeezed states saturate $\mathcal{J}^{(\text{ult})}$ with erasure noise, then an identical logical spin squeezed state saturates $\mathcal{J}^{(\text{ult})}$ in this case.

We remark that this protocol is a simpler alternative to other protocols in the literature [28] that convert the noise into an effective dephasing noise. In the effective dephasing protocol of Ref. [28] each logical qubit consists of one physical qubit with two noiseless ancillas. In the erasure conversion protocol, each logical qubit consists of two physical qubits without any noiseless ancillas. The erasure conversion protocol still requires sequential control, i.e., continuous erasure detection, but this can be accomplished via a continuous parity measurement [34, 36].

IV. OPTIMAL QUANTUM ERROR CORRECTION PROTOCOLS FOR $G \perp \sigma_z$

The protocols in this section involve continuous approximate quantum error correction and follow the general construction in Ref. [27]. In all protocols we define an error correction code $\{|0_L\rangle, |1_L\rangle\}$, which constitute a logical qubit. The probe is subject to continuous syndrome measurement and recovery operations. Let us denote the projection onto code space as $\Pi := |0_L\rangle\langle 0_L| + |1_L\rangle\langle 1_L|$, and the projection superoperator as $\mathcal{P}(\cdot) := \Pi(\cdot)\Pi$. The superoperator of the projection to the orthogonal complement of the code space is denoted by $\mathcal{P}_\perp := \mathbb{1} - \mathcal{P}$, and the recovery superoperator is denoted by \mathcal{R} . Hence a measurement and recovery channel of $\mathcal{P} + \mathcal{R}\mathcal{P}_\perp$ is sequentially applied to the probe. This channel leads to the following effective dynamics inside the code space [25, 27]

$$\frac{d\rho}{dt} = -i [\mathcal{P}(H), \rho] + \gamma_j \left(\mathcal{R}\mathcal{P}_\perp \left(L_j \rho L_j^\dagger \right) + \mathcal{P} \left(L_j \rho L_j^\dagger \right) + 1/2 \left\{ \mathcal{P} \left(L_j^\dagger L_j \right), \rho \right\} \right). \quad (\text{S1})$$

We therefore get an effective Hamiltonian of

$$H_{\text{eff}} = \mathcal{P}(H) = \begin{pmatrix} \langle 0_L | H | 0_L \rangle & \langle 0_L | H | 1_L \rangle \\ \langle 1_L | H | 0_L \rangle & \langle 1_L | H | 1_L \rangle \end{pmatrix}. \quad (\text{S2})$$

The dissipative part is also modified as shown in Eq. S1, where the non-Hermitian Hamiltonian becomes $\mathcal{P} \left(L_j^\dagger L_j \right)$, and the jump operators are dictated by $\mathcal{R}\mathcal{P}_\perp \left(L_j \rho L_j^\dagger \right) + \mathcal{P} \left(L_j \rho L_j^\dagger \right)$.

A. Optimal Heisenberg limit protocols for $G \perp \sigma_z$

As mentioned in the main text, for $G \perp \sigma_z$ HL can be achieved iff for every decay level e_j : $\min(\gamma_{1,j}, \gamma_{2,j}) = 0$. For all of these cases the noiseless QFI limit of $4N^2T^2$ is saturated using the following ancilla-free QEC code

$$\{|0_L\rangle = |+\rangle|+\rangle, |1_L\rangle = |-\rangle|-\rangle\}.$$

Let us show this using the effective dynamics of Eq. S2. The effective Hamiltonian is $H_{\text{eff}} = \mathcal{P}(H) = 2\omega\sigma_z^L$, where $\sigma_z^L = |0_L\rangle\langle 0_L| - |1_L\rangle\langle 1_L|$. The syndrome measurement is detecting whether any of the sensors decayed to the erasure states $\{|e_j\rangle\}_{j=1}^k$. The recovery operation is

$$\{|e_j\rangle|+\rangle, |+\rangle|e_j\rangle\} \rightarrow |+\rangle|+\rangle, \{|e_j\rangle|-\rangle, |-\rangle|e_j\rangle\} \rightarrow (-1)^{f_j} |-\rangle|-\rangle, \quad (\text{S3})$$

$$\text{where } f_j = \begin{cases} 1 & \gamma_{1,j} \geq \gamma_{2,j} \\ 2 & \text{otherwise.} \end{cases} \quad (\text{S4})$$

Formally, the recovery channel is given by

$$\begin{aligned} \mathcal{R}(\cdot) = \sum_j & \left(|0_L\rangle \langle e_j, + | + \langle +, e_j | \rangle + (-1)^{f_j} |1_L\rangle \langle e_j, - | + \langle -, e_j | \rangle \right) (\cdot) \\ & \left((|e_j, +\rangle + |+, e_j\rangle) \langle 0_L | + (-1)^{f_j} (|e_j, -\rangle + |-, e_j\rangle) \langle 1_L | \right). \end{aligned} \quad (\text{S5})$$

Observe that $\mathcal{P}(L_j^\dagger L_j) = \mathbb{1}$, $\mathcal{P}(L_j \rho L_j^\dagger) = 0$, $\mathcal{R} \mathcal{P}_\perp(L_j \rho L_j^\dagger) = \rho$. Hence the effective dynamics of Eq. S1 is the noiseless $\frac{d\rho}{dt} = -i2\omega [\sigma_z^L, \rho]$, such that the noiseless QFI $I = 4N^2 T^2 = 16T^2$ ($N = 2$ in this case) is retrieved.

More generally, for any N -qubit code space

$$\{|0_L\rangle = |+\rangle^N, |1_L\rangle = |-\rangle^N\},$$

the effective master equation is

$$\frac{d\rho}{dt} = -iN\omega [\sigma_z^L, \rho],$$

and thus the optimal noiseless QFI of $4N^2 T^2$ is achieved.

B. Optimal standard quantum limit protocols for $G \perp \sigma_z$

Let us consider the case of a single erasure state $|e\rangle$. As shown in the main text and in Appendix I the ultimate sequential bound is $\mathcal{J}^{(\text{ult})} = \frac{4}{\min\{\gamma_1, \gamma_2\}} NT$. Assuming without loss of generality that $\gamma_1 \leq \gamma_2$, we show that the optimal approximate QEC code is given by

$$\{|0_L\rangle = (\epsilon|1\rangle + \sqrt{1-\epsilon^2}|2\rangle) |0_a\rangle, |1_L\rangle = (\epsilon|1\rangle - \sqrt{1-\epsilon^2}|2\rangle) |1_a\rangle\} \text{ with } \epsilon \rightarrow 0,$$

such that $\mathcal{J}^{(\text{ult})}$ is asymptotically attainable using optimal logical spin squeezed state of this code. The recovery channel is given by

$$\mathcal{R}(\cdot) = (|0_L\rangle \langle e, 0_a | - |1_L\rangle \langle e, 1_a |) (\cdot) (|e, 0_a\rangle \langle 0_L | - |e, 1_a\rangle \langle 1_L |).$$

Let us now derive the effective dynamics. The effective Hamiltonian is (S2)

$$H_{\text{eff}} = \omega \begin{pmatrix} \langle 0_L | \sigma_x | 0_L \rangle & \langle 0_L | \sigma_x | 1_L \rangle \\ \langle 1_L | \sigma_x | 0_L \rangle & \langle 1_L | \sigma_x | 1_L \rangle \end{pmatrix} = \omega \begin{pmatrix} 2\epsilon\sqrt{1-\epsilon^2} & 0 \\ 0 & -2\epsilon\sqrt{1-\epsilon^2} \end{pmatrix}.$$

To derive the effective dissipative dynamics, note that

$$\begin{aligned} (i) \quad & \mathcal{P}(\gamma_2 \sigma_2^\dagger \sigma_2) = \gamma_2(1-\epsilon^2)\mathbb{1}, \quad \mathcal{P}(\gamma_1 \sigma_1^\dagger \sigma_1) = \gamma_1 \epsilon^2 \mathbb{1} \\ (ii) \quad & \mathcal{R} \circ \mathcal{P}_\perp(\gamma_2 \sigma_2 \rho \sigma_2^\dagger) = \gamma_2(1-\epsilon^2)\rho \\ (iii) \quad & \mathcal{R} \circ \mathcal{P}_\perp(\gamma_1 \sigma_1 \rho \sigma_1^\dagger) = \gamma_1 \epsilon^2 \sigma_z^L \rho \sigma_z^L, \end{aligned} \quad (\text{S6})$$

and $\mathcal{P}(\gamma_j \sigma_j \rho \sigma_j^\dagger) = 0$. (ii) follows from the fact that \mathcal{R} corrects the dominant σ_2 error, and (iii) is due to the fact that \mathcal{R} does not correct σ_1 errors and induces a σ_z^L error after the recovery.

Inserting Eq. S6 in Eq. S1 we obtain the following effective master equation

$$\frac{d\rho}{dt} = -i\omega \left[2\epsilon\sqrt{1-\epsilon^2} \sigma_z^L, \rho \right] + \gamma_1 \epsilon^2 (\sigma_z^L \rho \sigma_z^L - \rho). \quad (\text{S7})$$

We thus obtain an effective Hamiltonian of $\omega 2\epsilon\sqrt{1-\epsilon^2} \sigma_z^L$ and an effective dephasing noise of $D[\sqrt{\gamma_1 \epsilon} \sigma_z^L]$. For this dephasing model the sequential ECQFI is

$$\mathcal{J}^{(\text{ult})} = \frac{4\epsilon^2(1-\epsilon^2)}{\epsilon^2 \gamma_1} T = 4 \frac{1-\epsilon^2}{\gamma_1} T \xrightarrow{\epsilon \rightarrow 0} \frac{4T}{\gamma_1}.$$

It thus saturates the bound for $\epsilon \rightarrow 0$, and since it is dephasing, it is saturable by employing an appropriate logical spin squeezed state [28, 52]. Note that this optimal code corresponds to the limit of vanishing signal and vanishing noise.

V. SINGLE QUBIT ECQFI BOUNDS AND PROTOCOLS

We calculate the optimal product state QFI, $\mathfrak{J}_N^{(\text{prod})}$, using extended channel QFI (ECQFI) bounds. Given a quantum channel, \mathcal{E} , the ECQFI optimizes the QFI over all possible input states (including input states that have entanglement of the probe with a noiseless ancilla)

$$\mathcal{I}(\mathcal{E}) = \max_{\rho_0} I(\mathcal{E}(\rho_0)).$$

Let $\mathbf{K} = \{K\}_{i=1}^m$ be the $d_{in} \times d_{out}$ Kraus operators of the channel, the ECQFI is then given by the following minimization problem [20, 68]

$$4 \min_h \|\left(\dot{\mathbf{K}} - ih\mathbf{K}\right)^\dagger \left(\dot{\mathbf{K}} - ih\mathbf{K}\right)\|, \quad (\text{S1})$$

where the minimization is over all hermitian $m \times m$ h matrices. This problem can be recast as an SDP, denoting $\dot{\mathbf{K}} = \dot{\mathbf{K}} - ih\mathbf{K}$, the SDP reads [68]

$$I(\epsilon) = 4 \min_h \lambda, \quad \text{subject to} \quad \begin{pmatrix} \sqrt{\lambda} I_{d_{in}} & \dot{\mathbf{K}}^\dagger \\ \dot{\mathbf{K}} & \sqrt{\lambda} I_{m \cdot d_{out}} \end{pmatrix} \geq 0.$$

While in general the optimal input state may require entanglement with noiseless ancilla, we will show that this is not the case in our erasure noise problems. Therefore $\mathfrak{J}_N^{(\text{prod})}$ is given by

$$\mathfrak{J}_N^{(\text{prod})} = \max_t \frac{NT}{t} \mathcal{I}(\mathcal{E}(t))$$

A. $\mathfrak{J}_N^{(\text{prod})}$ for erasure qubits with $G \parallel \sigma_z$

Let us first consider the case of a single erasure state $|e\rangle$. The Kraus operators for an initial state with $d_{in} = 2$ are given by

$$\mathbf{K} = \left[\begin{pmatrix} \sqrt{\eta_1} e^{-i2\omega t} & 0 \\ 0 & \sqrt{\eta_2} \\ 0 & 0 \end{pmatrix}, \begin{pmatrix} 0 & 0 \\ 0 & 0 \\ \sqrt{1-\eta_1} & 0 \end{pmatrix}, \begin{pmatrix} 0 & 0 \\ 0 & 0 \\ 0 & \sqrt{1-\eta_2} \end{pmatrix} \right]^T,$$

where $\eta_1 = e^{-\gamma_1 t}$, $\eta_2 = e^{-\gamma_2 t}$. The derivatives

$$\dot{K}_1 = \begin{pmatrix} -2it\sqrt{\eta_1}e^{-2i\omega t} & 0 \\ 0 & 0 \\ 0 & 0 \end{pmatrix},$$

and the others are zero. The minimization problem of Eq. S1 can then be solved analytically. It is simple to see that the minimum is obtained for h that takes the form of $h = \begin{pmatrix} \lambda & 0 & 0 \\ 0 & 0 & 0 \\ 0 & 0 & 0 \end{pmatrix}$, with some $\lambda \in \mathbb{R}$. With this choice of h we have

$$\left(\dot{\mathbf{K}} - ih\mathbf{K}\right)^\dagger \left(\dot{\mathbf{K}} - ih\mathbf{K}\right) = \begin{pmatrix} (2t + \lambda)^2 \eta_1 & \\ & \lambda^2 \eta_2 \end{pmatrix}.$$

The minimum is obtained when $(2t + \lambda)^2 \eta_1 = \lambda^2 \eta_2$. This equation has two solutions: $\lambda = \frac{2t\sqrt{\eta_1}}{\sqrt{\eta_2} - \sqrt{\eta_1}}$, $-\frac{2t\sqrt{\eta_1}}{\sqrt{\eta_2} + \sqrt{\eta_1}}$, where the minimal operator norm is obtained for the latter: $\lambda = -\frac{2t\sqrt{\eta_1}}{\sqrt{\eta_2} + \sqrt{\eta_1}}$. The ECQFI is thus

$$\mathcal{I} = \frac{16t^2 \eta_1 \eta_2}{(\sqrt{\eta_1} + \sqrt{\eta_2})^2} = \frac{16t^2}{(e^{\gamma_1 t/2} + e^{\gamma_2 t/2})^2}. \quad (\text{S2})$$

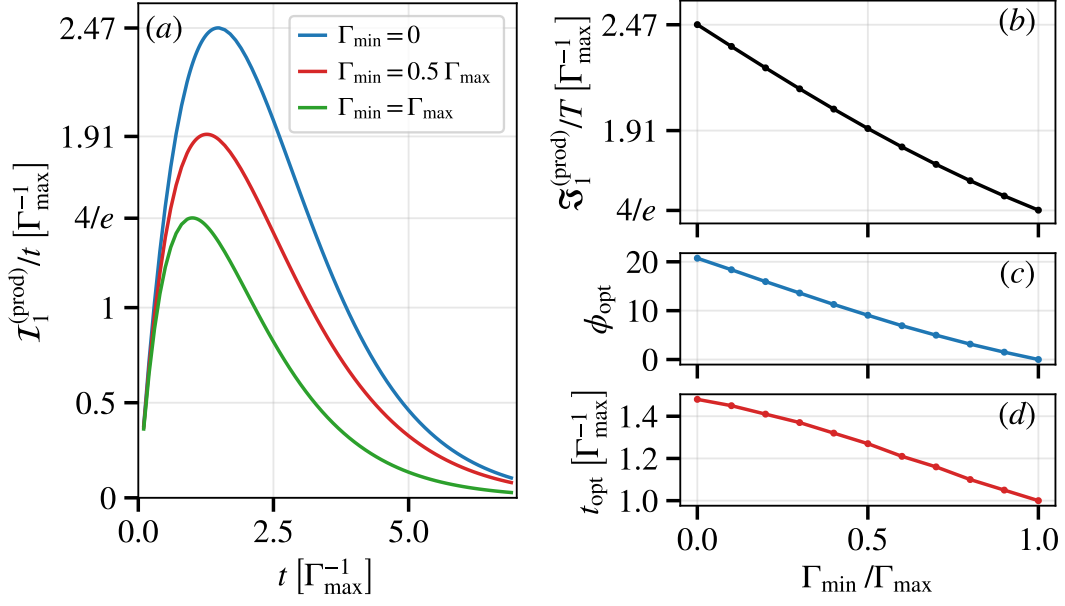


Figure S5: Single qubit ECQFI bounds and protocols for $G = \sigma_z$ for various erasure decay configurations. (a) ECQFI as a function of time for different Γ_{min} . (Eq. S3) (b) The t -optimized ECQFI as a function of $\Gamma_{\text{min}}/\Gamma_{\text{max}}$. (c) and (d) present the optimal protocol. (c) Optimal ϕ as a function of the ratio $\Gamma_{\text{min}}/\Gamma_{\text{max}}$. (Eq. S4) (d) Optimal measurement time, t_{opt} , as a function of $\Gamma_{\text{min}}/\Gamma_{\text{max}}$.

This ECQFI is validated with numerical SDP calculation for $\gamma_1 = 1$ and $\gamma_2 \in \{0, 0.5, 1\}$ and is plotted in Fig. S5.

We now generalize this analysis to an arbitrary number of erasure levels. In the multi-erasure case the Kraus operators are

$$\left\{ K_1 = e^{-\frac{t}{2}(4i\omega + \sum_j \gamma_{1,j})} |1\rangle \langle 1| + e^{-\frac{t}{2}(4i\omega + \sum_j \gamma_{2,j})} |2\rangle \langle 2| \right\} \cup \left\{ \sqrt{1 - e^{-\gamma_{1,j}t}} |e_j\rangle \langle 1|, \sqrt{1 - e^{-\gamma_{2,j}t}} |e_j\rangle \langle 2| \right\}_j.$$

Similar to the single erasure case only K_1 is non-zero. Addressing the optimization problem of Eq. S1 the optimal h

is $h_{i,j} = \begin{cases} \lambda & i = j = 1 \\ 0 & \text{otherwise} \end{cases}$ for some $\lambda \in \mathbb{R}$. We then obtain

$$\left(\dot{\mathbf{K}} - ih\mathbf{K} \right)^\dagger \left(\dot{\mathbf{K}} - ih\mathbf{K} \right) = \begin{pmatrix} (2t + \lambda)^2 e^{-\sum_j \gamma_{1,j}t} & \\ & \lambda^2 e^{-\sum_j \gamma_{2,j}t} \end{pmatrix}.$$

Minimizing the operator norm over λ leads to the ECQFI

$$\mathcal{I} = \frac{16t^2}{(e^{\Gamma_1 t/2} + e^{\Gamma_2 t/2})^2}, \quad (\text{S3})$$

which is the same as the single erasure state where $\gamma_1 \mapsto \Gamma_1, \gamma_2 \mapsto \Gamma_2$.

It should be noted that this ECQFI is the same as the one obtained with the following qubit thermal channel

$$\mathbf{K} = \left[\left(\begin{pmatrix} \sqrt{\eta_{s,1}} e^{-2i\omega t} & 0 \\ 0 & \sqrt{\eta_{s,2}} \end{pmatrix}, \begin{pmatrix} 0 & 0 \\ \sqrt{1 - \eta_{s,1}} & 0 \end{pmatrix}, \begin{pmatrix} 0 & \sqrt{1 - \eta_{s,2}} \\ 0 & 0 \end{pmatrix} \right)^T, \right.$$

with $\eta_{s,1} = e^{-\sum_j \gamma_{1,j}t}, \eta_{s,2} = e^{-\sum_j \gamma_{2,j}t}$. The reason for this is that by adding an ancillary noiseless qubit, the thermal channel is converted to our erasure noise channel while keeping the Hamiltonian the same.

The optimal initial state— For an initial state $\rho_0 = \frac{1}{2}(\mathbb{1} + \cos\phi\sigma_x + \sin\phi\sigma_z)$, the evolved state, obtained by solving the master equation, is

$$\rho(t) = \begin{pmatrix} \frac{1}{2}e^{-\gamma_1 t}(1 + \sin\phi) & \frac{1}{2}e^{-\frac{1}{2}t(\gamma_1 + \gamma_2 + 4i\omega)}\cos\phi & 0 \\ \frac{1}{2}e^{-\frac{1}{2}t(\gamma_1 + \gamma_2 - 4i\omega)}\cos\phi & \frac{1}{2}e^{-t\gamma_2}(1 - \sin\phi) & 0 \\ 0 & 0 & \frac{1}{2}e^{-t(\gamma_1 + \gamma_2)}[e^{\gamma_1 t}(2e^{t\gamma_2} + \sin\phi - 1) - e^{t\gamma_2}(1 + \sin\phi)] \end{pmatrix}.$$

The resulting QFI is:

$$I = \frac{8t^2 \cos^2\phi}{e^{\gamma_1 t}(1 - \sin\phi) + e^{t\gamma_2}(1 + \sin\phi)}.$$

Solving for the optimal ϕ yields

$$\sin\phi_{\text{opt}} = \tanh\frac{t\gamma_1}{4}\left(1 - \frac{\gamma_2}{\gamma_1}\right). \quad (\text{S4})$$

Inserting this ϕ_{opt} we obtain the ECQFI of Eq. S2. This optimal state can be also written as $|\psi_{\text{opt}}\rangle = \sqrt{p_{\text{opt}}}|1\rangle + \sqrt{1 - p_{\text{opt}}}|2\rangle$ with $p_{\text{opt}} = 1/2\left(1 + \tanh\frac{t_{\text{opt}}}{4}(\Gamma_1 - \Gamma_2)\right)$. This confirms that in this case the ECQFI is saturated without any noiseless ancilla. For multi-erasure case the same results are obtained where each γ_i is replaced by $\Gamma_i = \sum_j \gamma_{i,j}$.

Time optimized ECQFI— The ECQFI (Eq. S2) represents an optimization over all initial states. To obtain $\mathfrak{J}_N^{(\text{prod})}$ we need to further optimize this ECQFI over measurement time. Let us assume without loss of generality $\gamma_1 \leq \gamma_2$. If $\gamma_1 = 0$, the optimal time is

$$t_{\text{opt}} = \frac{1}{\gamma_2} \left[1 + 2W_0\left(\frac{1}{2\sqrt{e}}\right) \right] \approx \frac{1.48}{\gamma_2}, \quad (\text{S5})$$

where W_0 is the Lambert function. Hence, $\mathfrak{J}_N^{(\text{prod})}$ in this case is

$$\mathfrak{J}_N^{(\text{prod})} = \frac{64W_0^2\left(\frac{1}{2\sqrt{e}}\right)}{1 + 2W_0\left(\frac{1}{2\sqrt{e}}\right)} \frac{NT}{\gamma_2} \approx \frac{2.47NT}{\gamma_2}$$

For comparison, if the initial state ρ_0 is located at the equator of the Bloch sphere, which is the typical scenario in experiments, then $t_{\text{opt}} \approx 1.27\gamma_2^{-1}$ and $I \approx 2.22T/\gamma_2$. Thus, ϕ_{opt} improves the QFI by around 11%.

In the symmetric case of $\gamma_2 = \gamma_1$, we have $t_{\text{opt}} = \gamma_2^{-1}$ and $\mathfrak{J}_N^{(\text{prod})}$ is thus $\mathfrak{J}_N^{(\text{prod})} = 4NT/(\gamma_2 e)$.

For arbitrary γ_2, γ_1 , we solve numerically and the results are shown in Fig. S5.

B. $\mathfrak{J}_N^{(\text{prod})}$ for erasure qubits with $G \perp \sigma_z$

We show in this section that the single qubit QFI in this case is upper bounded by

$$I \leq \frac{16}{\max(\gamma_1, \gamma_2)} T = \frac{16}{\gamma_2} T, \quad (\text{S6})$$

where without loss of generality $\gamma_1 \leq \gamma_2$. To this end, we study the single qubit ECQFI of this problem for different values of $\omega, \gamma_1, \gamma_2$, and the relevant optimal protocols. This upper bound establishes the significant gain that can be obtained with QEC in this case (the QFI with QEC is given in S2). Let us first study the case of a single erasure noise $D(\sqrt{\gamma_2}\sigma_2)$ and show that the ECQFI in this case satisfies $I \leq \frac{16}{\gamma_2} T$, with equality when $\omega \rightarrow 0$.

Single erasure decay: Let us consider the case of a single Lindblad term of $\gamma_2(\sigma_2\rho\sigma_2^\dagger - 1/2\{\sigma_2^\dagger\sigma_2, \rho\})$. We compute the Kraus operators numerically, and use them to calculate the ECQFI with SDP. The ECQFI for different values of ω is shown in the Fig. S6 (solid lines). We observe from the numerical results that for every t the largest

ECQFI is obtained for $\omega \rightarrow 0$: $\mathcal{I}(\omega, t) \leq \mathcal{I}(\omega \rightarrow 0, t)$. Specifically, the t -optimized ECQFI lies within the range of $\frac{8}{\gamma_2 e} T \leq \mathfrak{I}_1^{(\text{prod})} \leq \frac{16}{\gamma_2} T$, where the upper bound is attainable in the limit of $\omega \ll \gamma_2$ and the lower bound corresponds to the limit of $\omega \gg \gamma_2$. The transition between the two regimes is shown in Fig. S6.

Given $\omega \ll \gamma_2$, the optimal initial state is $|\psi_0\rangle = |1\rangle$. The optimality of this state is intuitive since it does not suffer from erasure noise, only $|2\rangle$ decays to $|e\rangle$. With this initial state, the decay of the dynamics is induced from the coupling of $|1\rangle$ to $|2\rangle$ through H and the erasure noise of $|2\rangle$. This is thus a coupling mediated decay, and since $\omega \ll \gamma_2$ (because $\omega \rightarrow 0$), we can obtain an effective dynamics using the theory of adiabatic elimination [69–71]. The idea is that due to the fast decay of $|1\rangle$, we can adiabatically eliminate it and derive an effective dynamics that involves only the subspace of $\{|1\rangle, |e\rangle\}$. Using Eqs. (3), (4) of Ref. [69] we get that the effective jump operator is $L_{\text{eff}} = LH_{\text{NH}}^{-1}V_+$, where in our case $V_+ = \omega|2\rangle\langle 1|$, $H_{\text{NH}} = \frac{\gamma_2}{2}|2\rangle\langle 2|$, $L = \sqrt{\gamma_2}\sigma_2$, hence we obtain $L_{\text{eff}} = 2\frac{\omega}{\sqrt{\gamma_2}}\sigma_1$. The effective master equation is thus

$$\dot{\rho} = 4\frac{\omega^2}{\gamma_2} \left(\sigma_1 \rho \sigma_1^\dagger - 1/2 \left\{ \sigma_1^\dagger \sigma_1, \rho \right\} \right).$$

We show in Fig. S7 that this effective dynamics indeed fits the exact time evolution for $t \gg 1/\gamma_2$. The t -optimized ECQFI given this effective dynamics is $16T/\gamma_2$ [65, 66]. The numerical results of Fig. S6 confirm that this expression matches the t -optimized ECQFI obtained from the full dynamics.

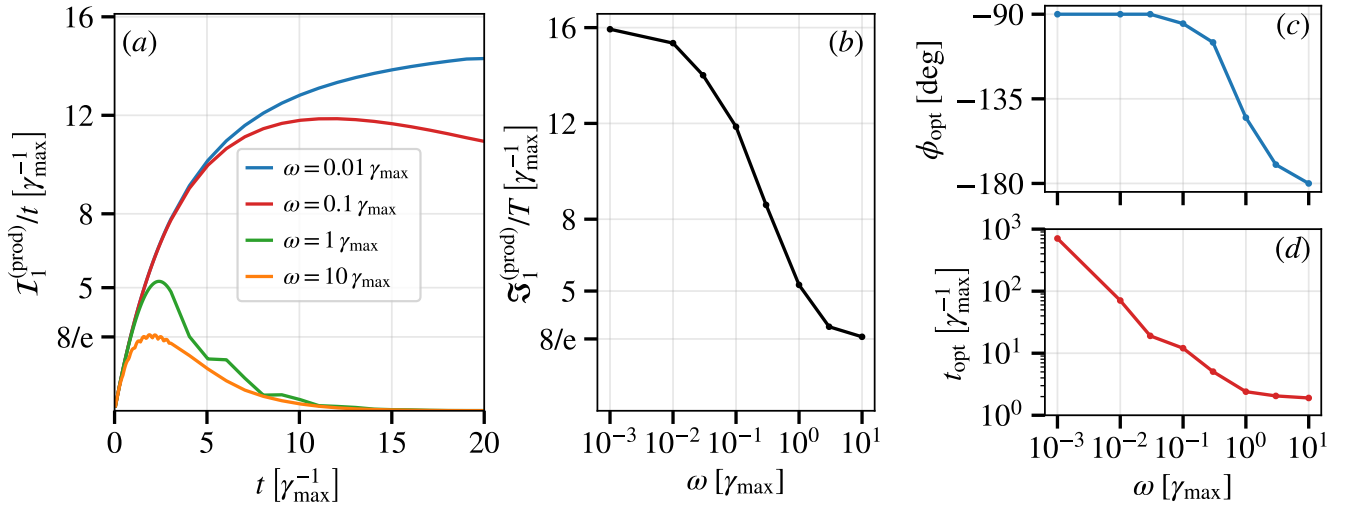


Figure S6: Single qubit ECQFI bounds and protocols for $G = \sigma_x$ and a single erasure decay configuration: $\gamma_{\text{min}} = 0$. (a) ECQFI as a function of time for different ω . (b) The t -optimized ECQFI as a function of ω . The optimal ECQFI rate is obtained as $\omega \rightarrow 0$, such that the t -optimized ECQFI converges to $16T/\gamma_{\text{max}}$ in this limit. (c) and (d) present the optimal protocol. (c) optimal ϕ as a function of ω . (d) optimal measurement time, t_{opt} as a function of ω .

Let us show this more explicitly and evaluate the optimal t needed to saturate t -optimized ECQFI. we solve the master equation given an initial state of $|\psi_0\rangle = |1\rangle$, and expand $\rho(t)$ to second order in ω/γ_1 . we find

$$\rho(t) = \begin{bmatrix} \frac{4\omega^2}{\gamma_2^2} + \frac{4\omega^2}{\gamma_2^2} e^{-t\gamma_2} - \frac{8\omega^2}{\gamma_2^2} e^{-\frac{t\gamma_2}{2}} & -\frac{2i\omega}{\gamma_2} + \frac{2i\omega}{\gamma_2} e^{-\frac{t\gamma_2}{2}} & 0 \\ \frac{2i\omega}{\gamma_2} - \frac{2i\omega}{\gamma_2} e^{-\frac{t\gamma_2}{2}} & 1 - \frac{4t\omega^2}{\gamma_2} + \frac{8\omega^2}{\gamma_2^2} - \frac{8\omega^2}{\gamma_2^2} e^{-\frac{t\gamma_2}{2}} & 0 \\ 0 & 0 & \frac{4t\omega^2}{\gamma_2} - \frac{12\omega^2}{\gamma_2^2} - \frac{4e^{-t\gamma_2}\omega^2}{\gamma_2^2} + \frac{16\omega^2}{\gamma_2^2} e^{-\frac{t\gamma_2}{2}} \end{bmatrix} + \mathcal{O}((\omega/\gamma_2)^3) \quad (\text{S7})$$

$$\approx^* \begin{bmatrix} \frac{4\omega^2}{\gamma_2^2} & -\frac{2i\omega}{\gamma_2} & 0 \\ \frac{2i\omega}{\gamma_2} & e^{-\frac{4t\omega^2}{\gamma_2}} + \frac{8\omega^2}{\gamma_2^2} & 0 \\ 0 & 0 & 1 - e^{-\frac{4t\omega^2}{\gamma_2}} - \frac{12\omega^2}{\gamma_2^2} \end{bmatrix}, \quad (\text{S8})$$

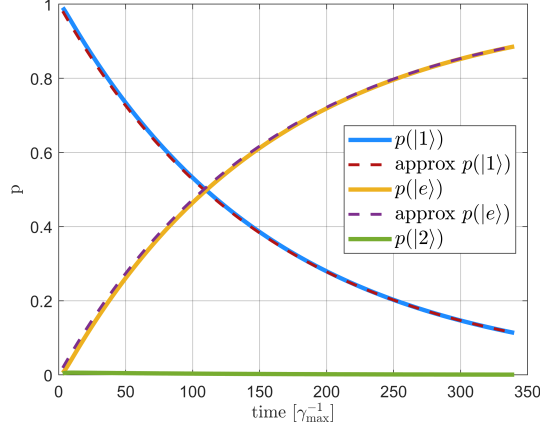


Figure S7: Measurement probabilities of $|1\rangle$, $|2\rangle$, and $|e\rangle$ as a function of time for a single erasure noise setting ($\gamma_1 = 0$), given an input state of $|1\rangle$. In this illustration $\omega = 0.04\gamma_2 \ll \gamma_2$. Dashed lines show the adiabatic elimination approximation, which agrees with the exact dynamics.

where in (*) we eliminated the terms that decay as $e^{-\gamma_2 t}$ and approximated $1 - \frac{4t\omega^2}{\gamma_2}$ by $e^{-\frac{4t\omega^2}{\gamma_2}}$. We can neglect in Eq. S8 all terms that go as ω^2/γ_2^2 and do not grow with t . We obtain that all $\{|2\rangle\langle j|, |j\rangle\langle 2|\}$ can be neglected such that we are left with the following effective state: $e^{-\frac{4t\omega^2}{\gamma_2}}|1\rangle\langle 1| + \left(1 - e^{-\frac{4t\omega^2}{\gamma_2}}\right)|e\rangle\langle e|$. This is exactly the adiabatic elimination approximation and the approximated probabilities in Fig. S7. Given this effective state the QFI is

$$I = \frac{(\partial_\omega p(|e\rangle))^2}{p(|e\rangle)} \approx \frac{64\omega^2 t^2 e^{-t\frac{8t\omega^2}{\gamma_2}}}{\gamma_2^2 \left(1 - e^{-\frac{4t\omega^2}{\gamma_2}}\right)} \underset{t \ll \gamma_2/\omega^2}{\approx} 16 \frac{t}{\gamma_2}, \quad (\text{S9})$$

which is the bound that we observe numerically. Eq. S9 also implies that this QFI is saturable by measuring the erasure state $|e\rangle$.

While the adiabatic elimination approximation suggests that the bound is achieved for any measurement time $t \ll \gamma/\omega^2$, the optimal time analysis is more subtle. To determine the optimal measurement time and the leading order correction to the QFI due to finite ω , we must also include the stationary term in $p(|e\rangle)$: $p(|e\rangle) = 1 - e^{-4t\frac{\omega^2}{\gamma_2}} - 12\omega^2/\gamma_2^2 + \mathcal{O}((\omega/\gamma_2)^3)$. Inserting this expression into the QFI calculation of Eq. S9 leads to $I \approx \frac{16t}{\gamma_2} - \frac{48}{\gamma_2^2}(1 + 2\omega^2 t^2) + \mathcal{O}((\omega/\gamma_2)^3)$. Optimizing I/t shows that the optimal measurement time is: $t = \frac{1}{\sqrt{2}\omega}$. The resulting t -optimized ECQFI, including the leading order correction in ω is: $\mathfrak{J}_1^{(\text{prod})} \approx \frac{16}{\gamma_2} T \left(1 - 6\sqrt{2}\frac{\omega}{\gamma_2}\right)$.

In the limit of $\omega \gg \gamma_2$, we observe that the t -optimized ECQFI equals to $8T/(\gamma_2 e)$ (see Fig. S6). In this limit the dynamics is equivalent to that of a symmetric erasure decay rate of $\gamma_2/2$, since the state rotates fast between $|2\rangle$ and $|1\rangle$ and thus experiences an effective symmetric erasure rate of $\gamma_2/2$. The t -optimized ECQFI in this symmetric case is $4T/(e\gamma_2/2) = 8T/(e\gamma_2)$, which explains the $\omega \gg \gamma_2$ limit.

Two erasure decays: Let us extend the analysis to the case of $\gamma_{\min} = \gamma_1 > 0$. We numerically calculate the ECQFI for $\omega = 0.001\gamma_{\max}, 0.01\gamma_{\max}, 0.1\gamma_{\max}$ and for different values γ_{\min} . The results are shown in Fig. S8. We want to consider the t -optimized ECQFI in the limit of $\omega, \gamma_{\min} \ll \gamma_{\max}$. Note that this expression depends on the order of limits. The behavior of the t -optimized ECQFI depends on ratio between ω^2/γ_{\max} and γ_{\min} . If γ_{\min} is small enough such that $\omega^2/\gamma_{\max} > \gamma_{\min}$ then the optimal QFI of $16T/\gamma_{\max}$ is retrieved. In the other limit of $\omega^2/\gamma_{\max} < \gamma_{\min}$, the QFI does not saturate this bound and converges to $\approx 5.6T/\gamma_{\max}$.

VI. CONTINUOUS ERASURE DETECTION PROTOCOLS

We derive the precision limits obtained with continuous erasure detection, i.e., by continuously detecting whether the qubit decayed to one of the erasure states and resetting the state accordingly. We remark that in these protocols

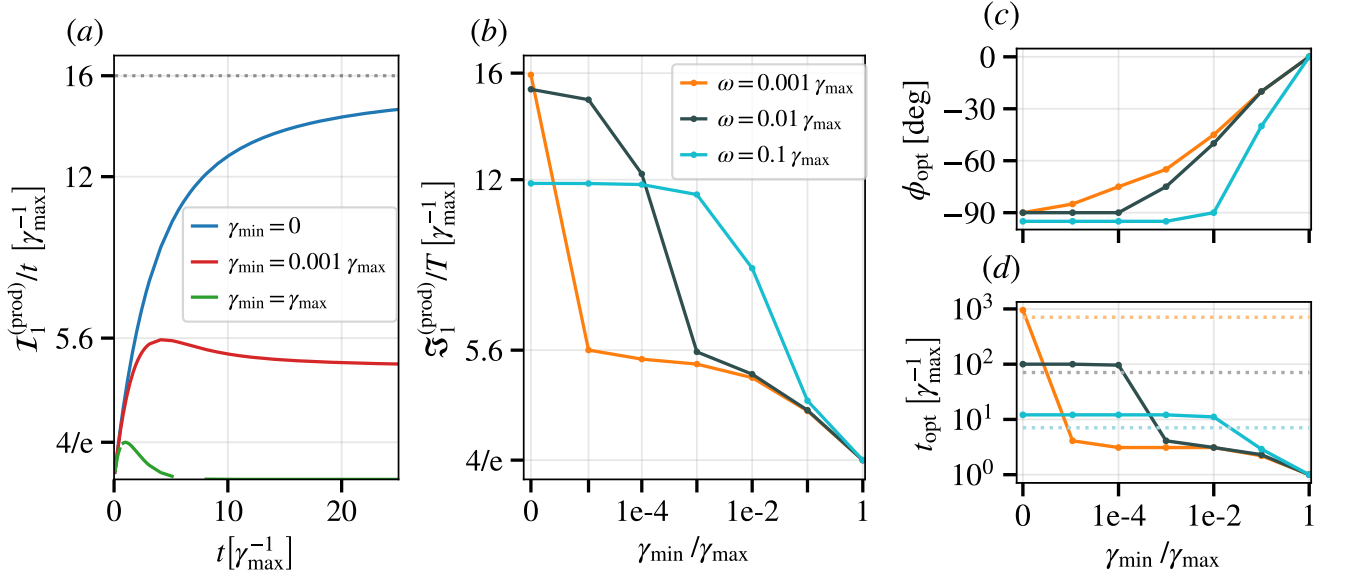


Figure S8: Single qubit ECQFI bounds and protocols for $G = \sigma_x$ for different $\gamma_{\min}/\gamma_{\max}$ in the small ω limit ($\omega \ll \gamma_{\max}$). (a) ECQFI as a function of time for $\omega = 0.01\gamma_{\max}$ and for different γ_{\min} . The t -optimized ECQFI ranges from $4T/(e\gamma_{\max})$ in the symmetric case of $\gamma_{\max} = \gamma_{\min}$ to $16T/\gamma_{\max}$ for $\gamma_{\min} = 0$. (b) The t -optimized ECQFI as a function of γ_{\min} for different values of ω . For $\gamma_{\min} < \omega^2/\gamma_{\max}$ the limit of $16T/\gamma_{\max}$ is achieved. For $\gamma_{\min} > \omega^2/\gamma_{\max}$ the t -optimized ECQFI converges to $5.6T/\gamma_{\max}$. (c) and (d) present the optimal protocol. (c) optimal ϕ as a function of the ratio $\gamma_{\min}/\gamma_{\max}$. (d) optimal measurement time, t_{opt} as a function of $\gamma_{\min}/\gamma_{\max}$. Dashed lines indicate $t_{\text{opt}} = \frac{1}{\sqrt{2}\omega}$, the small- ω limit at $\gamma_{\min} = 0$.

no entanglement or ancillary qubits are used, and the only assumptions are: 1. ability to perform continuous erasure detection. 2. ability to perform a fast reset of the state.

The optimal continuous erasure protocols depend on G , hence we split into the two cases of $G \parallel \sigma_z$ or $G \perp \sigma_z$, and analyze several continuous erasure detection strategies.

A. $\mathcal{J}_N^{(\text{cd})}$ for erasure qubits with $G \parallel \sigma_z$

Strategy 1: fixed τ after decay: In this strategy we initialize the qubit to a state $|\psi_0\rangle = \alpha|1\rangle + \beta|2\rangle$ and let it evolve, where the erasure states are being continuously detected. If an erasure is detected we reset the state to $|\psi_0\rangle$. In this case we lose the information about ω that was encoded in the qubit. If no erasure has been detected by time τ since the last reset, we perform an optimal measurement on the qubit. This measurement provides the information about ω . The analysis in this section assumes for simplicity a single erasure state with decay rates γ_1, γ_2 . The generalization to multi-erasure states is immediate: γ_i just needs to be replaced by $\Gamma_i = \sum_j \gamma_{i,j}$.

Let us first calculate the FI obtained with this strategy for the identical erasure rates case $\gamma := \gamma_1 = \gamma_2$. In this case the optimal initial state is $|\psi_0\rangle = \frac{1}{\sqrt{2}}(|1\rangle + |2\rangle)$, and the FI is given by

$$I = N_{\text{cycles}} p(\text{success}) 4\tau^2, \quad (\text{S1})$$

where N_{cycles} is the number of independent experiments (each one terminated by either decay or qubit measurement) and $p(\text{success})$ is the probability that no decay occurred in the cycle. Note that $p(\text{success}) = e^{-\gamma\tau}$, since the decay corresponds to a Poisson process with decay rate γ . In the limit of $T \rightarrow \infty$, $N_{\text{cycles}} \rightarrow \frac{T}{\langle\tau_{\text{cycle}}\rangle}$, where $\langle\tau_{\text{cycle}}\rangle$ is the average cycle time. $\langle\tau_{\text{cycle}}\rangle$ is given by

$$\langle\tau_{\text{cycle}}\rangle = e^{-\gamma\tau}\tau + \int_0^{\tau_{\text{meas}}} te^{-\gamma t}\gamma dt = \frac{1 - e^{-\gamma\tau}}{\gamma}. \quad (\text{S2})$$

Inserting Eq. S2 in Eq. S1, using $N_{\text{cycles}} \rightarrow \frac{T}{\langle \tau_{\text{cycle}} \rangle}$, we obtain

$$I = \frac{\gamma T}{1 - e^{-\gamma\tau}} e^{-\gamma\tau} 4\tau^2. \quad (\text{S3})$$

Optimizing over τ we obtain

$$\max_{\tau} \frac{\gamma T}{1 - e^{-\gamma\tau}} e^{-\gamma\tau} 4\tau^2 \approx \boxed{\frac{2.6}{\gamma} T}. \quad (\text{S4})$$

This FI expression can be proven rigorously using the renewal-reward theorem [72]. Let us define the random variables $(X_n, R_n)_n$, where X_n is the duration of the n -th cycle and R_n is the FI obtained from this cycle

$$R_n = \begin{cases} 4\tau^2 & X_n = \tau \\ 0 & X_n < \tau. \end{cases}$$

Both $(X_n)_n$ and $(R_n)_n$ are i.i.d random variables with averages $\langle R_j \rangle = e^{-\gamma\tau} 4\tau^2$, $\langle X_j \rangle = \langle \tau_{\text{cycle}} \rangle = \frac{1 - e^{-\gamma\tau}}{\gamma}$. Hence according to the renewal-reward theorem [72]

$$\lim_{T \rightarrow \infty} \frac{\sum_n R_n}{T} \rightarrow \frac{\langle R_j \rangle}{\langle X_j \rangle} = \frac{\gamma}{1 - e^{-\gamma\tau}} e^{-\gamma\tau} 4\tau^2,$$

which is the QFI rate of Eq. S3.

Let us generalize this to the case of unequal erasure decay rates. This analysis requires also optimization over the input state. Without loss of generality we can assume that the optimal input is on the $\sigma_x - \sigma_z$ plane: $|\psi_0\rangle = \cos(\pi/4 - \phi/2)|1\rangle + \sin(\pi/4 - \phi/2)|2\rangle$, where the optimal ϕ will be found later. Let us calculate the average cycle time and average FI per cycle. The probability of having no decay until time t is $\cos(\pi/4 - \phi/2)^2 e^{-\gamma_1 t} + \sin(\pi/4 - \phi/2)^2 e^{-\gamma_2 t}$, and the probability of decaying at time t is $\cos(\pi/4 - \phi/2)^2 e^{-\gamma_1 t} \gamma_1 dt + \sin(\pi/4 - \phi/2)^2 e^{-\gamma_2 t} \gamma_2 dt$. Hence the average cycle time is

$$\begin{aligned} \langle \tau_{\text{cycle}} \rangle &= \left(\cos(\pi/4 - \phi/2)^2 e^{-\gamma_1 \tau} + \sin(\pi/4 - \phi/2)^2 e^{-\gamma_2 \tau} \right) \tau \\ &+ \int_0^\tau t \left(\cos(\pi/4 - \phi/2)^2 e^{-\gamma_1 t} \gamma_1 + \sin(\pi/4 - \phi/2)^2 e^{-\gamma_2 t} \gamma_2 \right) dt = \\ &= \frac{(1 - e^{-\gamma_2 \tau})}{\gamma_2} \sin(\pi/4 - \phi/2)^2 + \frac{(1 - e^{-\gamma_1 \tau})}{\gamma_1} \cos(\pi/4 - \phi/2)^2. \end{aligned}$$

Let us now calculate the average FI per cycle. The QFI given a successful cycle is

$$I_{\text{cycle}} = 4\tau^2 \frac{e^{-(\gamma_1 + \gamma_2)\tau} \cos^2(\phi)}{\left(e^{-\gamma_2 \tau} \sin(\pi/4 - \phi/2)^2 + e^{-\gamma_1 \tau} \cos(\pi/4 - \phi/2)^2 \right)^2}.$$

The average FI per cycle is thus

$$p(\text{success}) I_{\text{cycle}} = 4\tau^2 \frac{e^{-(\gamma_1 + \gamma_2)\tau} \cos^2(\phi)}{e^{-\gamma_2 \tau} \sin(\pi/4 - \phi/2)^2 + e^{-\gamma_1 \tau} \cos(\pi/4 - \phi/2)^2}.$$

The total FI is thus

$$I = 4\tau^2 T \frac{e^{-(\gamma_1 + \gamma_2)\tau} 4p(1-p)}{\left(e^{-\gamma_2 \tau} (1-p) + e^{-\gamma_1 \tau} p \right) \left(\frac{(1 - e^{-\gamma_2 \tau})}{\gamma_2} (1-p) + \frac{(1 - e^{-\gamma_1 \tau})}{\gamma_1} p \right)}, \quad (\text{S5})$$

where we denoted $p = \cos(\pi/4 - \phi/2)^2$, $1 - p = \sin(\pi/4 - \phi/2)^2$ for brevity. With this notation $|\psi_0\rangle = \sqrt{p}|1\rangle + \sqrt{1-p}|2\rangle$. The optimal FI is then obtained by optimizing over p and τ .

Optimizing over p (for any τ) yields

$$p_{\text{opt}} = \frac{1}{1 + \sqrt{\frac{l_1 m_1}{l_2 m_2}}}, \quad (\text{S6})$$

where $l_i = e^{-\gamma_i \tau}$, $m_i = (1 - e^{-\gamma_i \tau})/\gamma_i$. Inserting this p_{opt} into Eq. S5 we obtain

$$I = 16\tau^2 T \frac{\sqrt{\frac{\int_0^\tau e^{\gamma_1 t} dt}{\int_0^\tau e^{\gamma_2 t} dt}}}{\left(1 + \sqrt{\frac{\int_0^\tau e^{\gamma_1 t} dt}{\int_0^\tau e^{\gamma_2 t} dt}}\right) \left(\int_0^\tau e^{\gamma_1 t} dt + \sqrt{\int_0^\tau e^{\gamma_1 t} dt} \sqrt{\int_0^\tau e^{\gamma_2 t} dt}\right)} \quad (\text{S7})$$

$$= \frac{16\tau^2 T}{\left(\sqrt{\int_0^\tau e^{\gamma_1 t} dt} + \sqrt{\int_0^\tau e^{\gamma_2 t} dt}\right)^2}.$$

$\mathfrak{J}_N^{(\text{cd})}$ is then obtained by optimizing this expression over τ , which matches the expression in the main text. This bound has the same functional form as the single-qubit ECQFI (Eq.S3), but with effectively reduced decay rates. To see this, note that the single qubit ECQFI is retrieved by replacing $\int_0^\tau e^{\gamma_j t} dt/\tau$ with $e^{\gamma_j \tau}$. We therefore obtain effective decay rates of $\log(\int_0^\tau e^{\gamma_j t} dt/\tau)$. Since $\int_0^\tau e^{\gamma_j t} dt/\tau \leq e^{\gamma_j \tau}$ the effective decay rate is indeed smaller than the original decay rate γ_j . The optimal values of p, τ and the resulting FI are shown in Fig. S9.

Strategy 2: fixed τ : This strategy underperforms strategy 1, but we provide it here for completeness. In this strategy we divide the experiment into periods of τ , where at the end of every such period the qubit is being measured in the optimal basis. Unlike the previous strategy, here the measurement is done in constant, predetermined time lapses. This strategy also leads to a considerable improvement compared to the ECQFI, yet it underperforms strategy 1. Let us calculate the optimal QFI with this strategy for the case of $\gamma := \gamma_1 = \gamma_2$. In this case the optimal initial state is $|\psi\rangle = \frac{1}{\sqrt{2}}(|1\rangle + |2\rangle)$ due to the identical decay rates. The FI given a total time T is

$$I = \frac{T}{\tau} I_\tau, \quad (\text{S8})$$

where I_τ is the FI obtained with this protocol given that the measurement time is τ . I_τ includes all possible trajectories, i.e., all possible outcomes of the erasure measurements and the final qubit measurement at τ . Let us denote the outcomes of the erasure measurements as \vec{x}_e and the outcome of the final qubit measurement as x_q . I_τ then equals to

$$I_\tau = \sum_{\vec{x}_e, x_q} \frac{(\partial_\omega p(\vec{x}_e, x_q))^2}{p(\vec{x}_e, x_q)} = \sum_{\vec{x}_e} p(\vec{x}_e) \sum_{x_q} \frac{(\partial_\omega p(x_q|\vec{x}_e))^2}{p(x_q|\vec{x}_e)},$$

where the last equality is due to the fact that $p(\vec{x}_e)$ is independent of ω and thus $\partial_\omega p(\vec{x}_e, x_q) = p(\vec{x}_e) \partial_\omega p(x_q|\vec{x}_e)$. It can be seen that the term $\sum_{x_q} \frac{(\partial_\omega p(x_q|\vec{x}_e))^2}{p(x_q|\vec{x}_e)}$ depends only on the latest time in which the qubit decayed. Denoting this time as t_{last} we have that

$$\sum_{x_q} \frac{(\partial_\omega p(x_q|\vec{x}_e))^2}{p(x_q|\vec{x}_e)} = 4(\tau - t_{\text{last}})^2$$

$$\Rightarrow I_\tau = \sum_{\vec{x}_e} p(\vec{x}_e) 4(\tau - t_{\text{last}}(\vec{x}_e))^2$$

The probability for a trajectory with k decays, where the last decay is at a fixed time t_{last} (t_1, \dots, t_{k-1} represent the other decay times) is

$$p(k \text{ decays}, t_k = t_{\text{last}}) = \gamma dt_{\text{last}} e^{-\gamma \tau} \int_0^{t_{\text{last}}} \gamma dt_{k-1} \dots \int_0^{t_3} \gamma dt_2 \int_0^{t_2} \gamma dt_1 =$$

$$\gamma dt_{\text{last}} e^{-\gamma \tau} \frac{(\gamma t_{\text{last}})^{k-1}}{(k-1)!}.$$

Hence the FI from all trajectories with k decays is

$$\gamma e^{-\gamma \tau} \int_0^\tau \frac{(\gamma t_{\text{last}})^{k-1}}{(k-1)!} 4(\tau - t_{\text{last}})^2 dt_{\text{last}} = \frac{8}{(\gamma)^2} e^{-\gamma \tau} \frac{(\gamma \tau)^{k+2}}{(k+2)!}$$

I_τ obtained by summing over all trajectories is thus

$$I_\tau = \frac{8}{(\gamma)^2} e^{-\gamma\tau} \sum_{k=0}^{\infty} \frac{(\gamma\tau)^{k+2}}{(k+2)!} = \frac{8}{(\gamma)^2} e^{-\gamma\tau} [e^{\gamma\tau} - (\gamma\tau + 1)].$$

We now want to optimize I (Eq. S8) over τ which leads to

$$\max_{\tau} \frac{8}{\gamma} \frac{1}{\gamma\tau} [1 - e^{-\gamma\tau} (\gamma\tau + 1)] T \approx \boxed{\frac{2.4}{\gamma} T}.$$

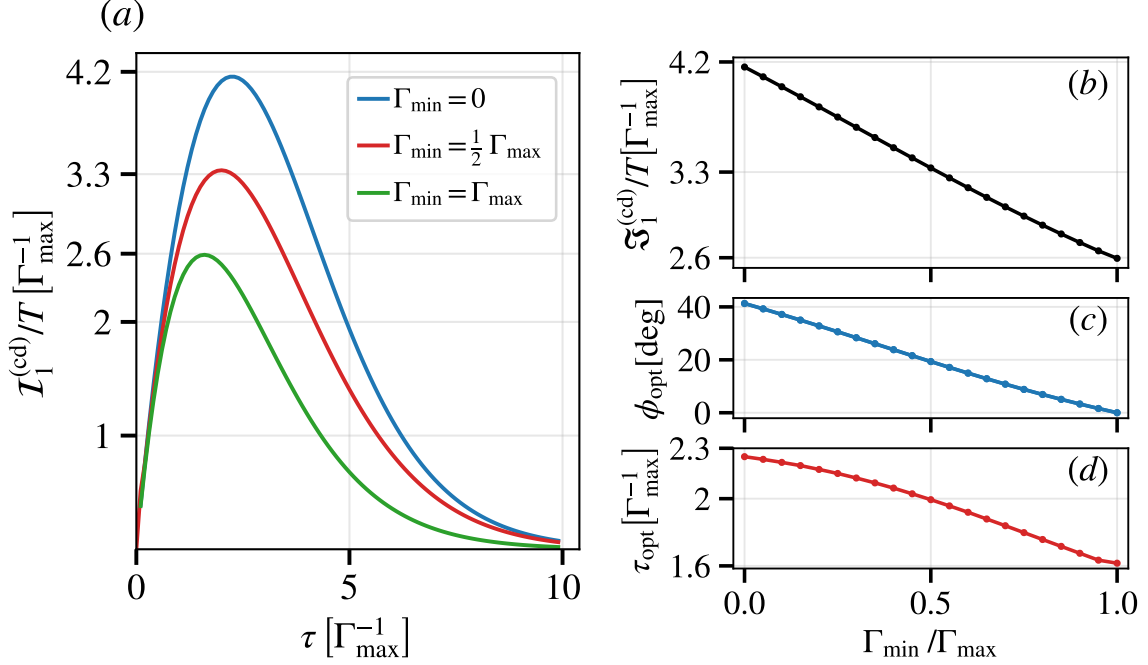


Figure S9: QFI achieved with continuous erasure detection strategy (strategy 1: fixed τ after measurement) for $G = \sigma_z$ and different values of Γ_{\min} (Eq. S7). (a) Continuous erasure detection QFI rate as a function of τ for different $\Gamma_{\min}, \Gamma_{\max}$. (b) QFI rate achieved with this continuous erasure strategy for different $\Gamma_{\min}/\Gamma_{\max}$. (c) and (d) present the optimal protocol: optimal initial state (ϕ_{opt} , extracted from S6) and optimal evolution time since the last decay τ .

Continuous erasure detection with entangled multi-probe strategies: Combining continuous erasure detection with entangled states is expected to lead to improved FI, i.e., FI larger than the product state bound of Eq. S4. We focus in this part on the equal decay rates case $\gamma := \gamma_1 = \gamma_2$. We first show that with GHZ states we obtain the same product state bound of Eq. S4 and cannot surpass it. We then show an example of an optimized entangled two-qubits protocol that obtains $I \approx \frac{2.72}{\gamma} T$ and thus surpasses this bound.

Let us show that GHZ states with continuous erasure detection lead to the same bound as product states with continuous erasure detection. Given a GHZ state $\frac{1}{\sqrt{2}} (|1\rangle^N + |2\rangle^N)$, Using strategy 1, the average FI per cycle is $e^{-N\gamma\tau} 4N^2\tau^2$ and the average cycle time is $\frac{1-e^{-N\gamma\tau}}{N\gamma}$. Defining $\gamma' = N\gamma$ we obtain that the FI is given by

$$I = N^2 \frac{T}{1 - e^{-\gamma'\tau}} e^{-\gamma'\tau} 4\gamma'\tau^2.$$

The optimization over τ is thus identical to Eq. S4 with replacing γ with $\gamma' = N\gamma$ and a global factor of N^2 leading to

$$\max_{\tau} N^2 \frac{T}{1 - e^{-\gamma'\tau}} e^{-\gamma'\tau} 4\gamma'\tau^2 T \approx N \frac{2.6}{\gamma} T, \quad (\text{S9})$$

which is the same bound as Eq. S4. Hence GHZ states are not optimal with this protocol and a more thorough optimization over the state and the strategy are required.

We consider state optimization for $N = 2$ qubits. From symmetry, we can restrict ourselves to states that take the form of

$$|\psi_0\rangle = \frac{\cos(\theta)}{\sqrt{2}}(|11\rangle + |22\rangle) + \frac{\sin(\theta)}{\sqrt{2}}(|12\rangle + |21\rangle).$$

Let us calculate the average FI per cycle. If no decay occurred until τ we obtain the FI $4\text{var}_{|\psi_0\rangle}(\sigma_{z,1} + \sigma_{z,2}) = 16 \cos(\theta)^2 \tau^2$. If a decay occurred in one of the qubits we immediately measure the remaining qubit in its optimal basis and reset the two qubits afterwards. The FI obtained after a decay is thus $4 \sin(2\theta) t^2$. The average FI per cycle is thus

$$e^{-2\gamma\tau} \tau^2 16 \cos(\theta)^2 + 4 \sin(2\theta) \int_0^\tau t^2 e^{-2\gamma t} 2\gamma dt = e^{-2\gamma\tau} \tau^2 16 \cos(\theta)^2 + \frac{2 \sin(2\theta)}{\gamma^2} [1 - e^{-2\gamma\tau} (1 + 2\gamma\tau + 2\gamma^2 \tau^2)].$$

The average cycle time is $\langle \tau_{\text{cycle}} \rangle = \frac{1 - e^{-2\gamma\tau}}{2\gamma}$. We thus want to optimize

$$\frac{e^{-2\gamma\tau} \tau^2 16 \cos(\theta)^2 + \frac{2 \sin(2\theta)}{\gamma^2} [1 - e^{-2\gamma\tau} (1 + 2\gamma\tau + 2\gamma^2 \tau^2)]}{\frac{1 - e^{-2\gamma\tau}}{2\gamma}}$$

over τ . This optimization yields $I \approx \frac{2.72}{\gamma} T$. This FI is indeed larger than the product state bound of Eq. S4. Combining larger N entanglement with continuous erasure detection should lead to further improvement and to faster convergence with N to the asymptotic sequential bound of $4T/\gamma$. We leave this analysis for future work.

B. $\mathfrak{J}_N^{(\text{cd})}$ for erasure qubits with $G \perp \sigma_z$

We focus on the single erasure noise decay. Without loss of generality, let $\gamma_1 = 0$. and $\gamma := \gamma_2$. We consider again strategy 1, fixed τ after reset, that was described earlier. Unlike the $G = \sigma_z$ case, now the decay vs. no-decay events provide information about ω . The optimal protocol employs the input state $|\psi_0\rangle = |1\rangle$, i.e., the noiseless state in the $\omega = 0$ limit, and $\tau \rightarrow \infty$. Hence in this case the protocol consists of the following repeated cycles: initialize the state in $|\psi_0\rangle = |1\rangle$, let it evolve with continuous erasure detection, wait until an erasure is detected and reset the state. We show that this protocol yields $I = 16T/\gamma$ for every ω .

Let us denote the probability density function of the decay time as $p_{\text{dec}}(t)$. Given the input state $|\psi_0\rangle = |1\rangle$ we have

$$p_{\text{dec}}(t) = \gamma \rho_{2,2}(t) = \frac{16e^{-\frac{t\gamma}{2}} \gamma \omega^2 \sinh^2\left(\frac{t}{4} \sqrt{\gamma^2 - 16\omega^2}\right)}{\gamma^2 - 16\omega^2}.$$

Using the renewal-reward theory we get that the total FI equals to: $I = \frac{T}{\langle \tau_{\text{cycle}} \rangle} I_{\text{cycle}}$, where I_{cycle} is the FI per cycle and $\langle \tau_{\text{cycle}} \rangle$ is the average time of a cycle. In this case

$$I_{\text{cycle}} = \int_0^\infty \frac{(\partial_\omega p_{\text{dec}}(t))^2}{p_{\text{dec}}(t)} dt = \frac{4\gamma^2 + 32\omega^2}{\omega^2 \gamma^2},$$

$$\langle \tau_{\text{cycle}} \rangle = \int_0^\infty t p_{\text{dec}}(t) dt = \frac{\gamma^2 + 8\omega^2}{4\omega^2 \gamma}.$$

Therefore

$$I = \frac{T}{\langle \tau_{\text{cycle}} \rangle} I_{\text{cycle}} = \frac{16}{\gamma} T.$$

Continuous erasure detection provides a modest improvement compared to the product protocols in this case: while product-state protocols require asymptotically small ω to reach this limit, this protocol achieves it for any ω .

Finite τ analysis: In the analysis above we chose $\tau \rightarrow \infty$. The optimality of this protocol is illustrated in Fig. S10, where the FI is plotted as a function of τ . Let us prove the optimality of $\tau \rightarrow \infty$. To this end, we calculate the FI as a function of τ . For any finite τ the protocol is: reset after any erasure, if no erasure occurred for a period of τ since the last reset, perform optimal measurement on the qubit and reset the state. The outcomes of each cycle are thus: {decay at $t < \tau$, no decay until τ followed by a qubit measurement}. The probability of no decay until τ is $p_{\text{nodec}}(\tau) = \rho_{1,1}(\tau) + \rho_{2,2}(\tau) = \frac{e^{-\frac{\tau}{2}} \left(-16\omega^2 + \gamma^2 \cosh\left(\frac{\tau}{2} \sqrt{\gamma^2 - 16\omega^2}\right) + \gamma \sqrt{\gamma^2 - 16\omega^2} \sinh\left(\frac{\tau}{2} \sqrt{\gamma^2 - 16\omega^2}\right) \right)}{\gamma^2 - 16\omega^2}$. Hence the probabilities of the different outcomes are $\{p_{\text{dec}}(t)\}_{t < \tau} \cup \{p_{\text{nodec}}(\tau) p_1, p_{\text{nodec}}(\tau) p_2\}$, where $\{p_1, p_2\}$ are the outcomes of the optimal qubit measurement. The FI per cycle is thus:

$$I_{\text{cycle}} = \int_0^\tau \frac{(\partial_\omega p_{\text{dec}}(t))^2}{p_{\text{dec}}(t)} dt + \frac{(\partial_\omega p_{\text{nodec}}(\tau))^2}{p_{\text{nodec}}(\tau)} + p_{\text{nodec}}(\tau) I_{\text{no-decay}}, \quad (\text{S10})$$

where $I_{\text{no-decay}}$ is the QFI of the qubit state conditioned on no decay until τ . The average time of a cycle is now

$$\tau_{\text{cycle}} = \int_0^\tau t p_{\text{dec}}(t) dt + p_{\text{nodec}}(\tau) \tau. \quad (\text{S11})$$

The total FI is given by $I = \frac{I_{\text{cycle}}}{\tau_{\text{cycle}}} T$. The numerical results of this calculation are shown in Fig. S10

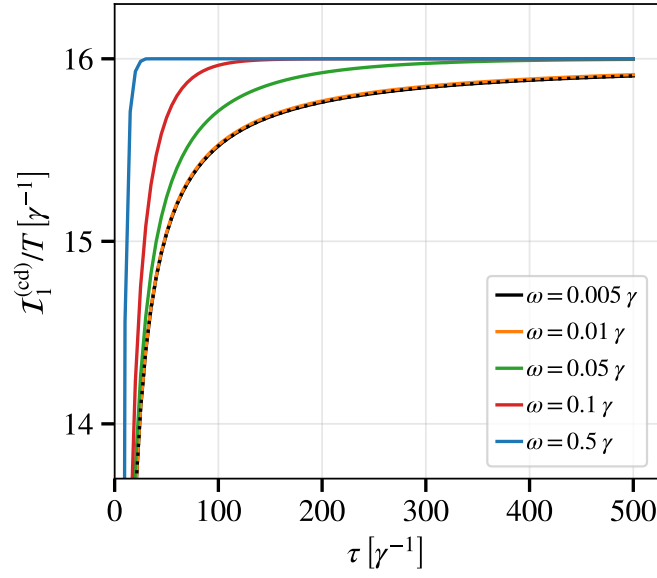


Figure S10: FI achieved with continuous erasure detection strategy for $G = \sigma_x$ with single erasure noise, i.e., $\gamma_{\text{min}} = 0$ and $\gamma_{\text{max}} \equiv \gamma$, for different values of ω . For every ω , $\tau_{\text{opt}} \rightarrow \infty$ and $\mathcal{I}_1^{(\text{cd})} = \frac{16T}{\gamma}$.

* arieli.michal@gmail.com

† tuvia.gefen@mail.huji.ac.il

- [1] Andrew D. Ludlow, Martin M. Boyd, Jun Ye, E. Peik, and P. O. Schmidt, “Optical atomic clocks,” *Rev. Mod. Phys.* **87**, 637–701 (2015).
- [2] John M Robinson, Maya Miklos, Yee Ming Tso, Colin J Kennedy, Tobias Bothwell, Dhruv Kedar, James K Thompson, and Jun Ye, “Direct comparison of two spin-squeezed optical clock ensembles at the 10- 17 level,” *Nature Physics* **20**, 208–213 (2024).
- [3] Raphael Kaubruegger, Denis V Vasilyev, Marius Schulte, Klemens Hammerer, and Peter Zoller, “Quantum variational optimization of ramsey interferometry and atomic clocks,” *Physical review X* **11**, 041045 (2021).
- [4] Raphael Kaubruegger and Adam M Kaufman, “Progress in quantum metrology and applications for optical atomic clocks,” arXiv preprint arXiv:2512.02202 (2025).
- [5] Timm Kielinski and Klemens Hammerer, “Bayesian frequency metrology with optimal ramsey interferometry in optical atomic clocks,” *Reports on Progress in Physics* **88**, 124001 (2025).
- [6] Su Direkci, Ran Finkelstein, Manuel Endres, and Tuvia Gefen, “Heisenberg-limited bayesian phase estimation with low-depth digital quantum circuits,” *npj Quantum Information* (2026).
- [7] Simon Schmitt, Tuvia Gefen, Felix M Stürner, Thomas Unden, Gerhard Wolff, Christoph Müller, Jochen Scheuer, Boris Naydenov, Matthew Markham, Sebastien Pezzagna, *et al.*, “Submillihertz magnetic spectroscopy performed with a nanoscale quantum sensor,” *Science* **356**, 832–837 (2017).
- [8] Jens M Boss, KS Cujia, Jonathan Zopes, and Christian L Degen, “Quantum sensing with arbitrary frequency resolution,” *science* **356**, 837–840 (2017).
- [9] Yifan Wang, Wenzhe Zhang, Haotian Chai, Zhenlin Zhang, Shaochun Lin, Xi Qin, and Jiangfeng Du, “Fully integrated quantum magnetometer based on nitrogen-vacancy centers,” *Phys. Rev. Appl.* **23**, 034008 (2025).
- [10] K. Herb, L. A. Völker, J. M. Abendroth, N. Meinhardt, L. van Schie, P. Gambardella, and C. L. Degen, “Quantum magnetometry of transient signals with a time resolution of 1.1 nanoseconds,” *Nature Communications* **16**, 822 (2025).
- [11] Nabeel Aslam, Matthias Pfender, Philipp Neumann, Rolf Reuter, Andrea Zappe, Felipe Fávoro de Oliveira, Andrej Denisenko, Hitoshi Sumiya, Shinobu Onoda, Junichi Isoya, *et al.*, “Nanoscale nuclear magnetic resonance with chemical resolution,” *Science* **357**, 67–71 (2017).
- [12] David R Glenn, Dominik B Bucher, Junghyun Lee, Mikhail D Lukin, Hongkun Park, and Ronald L Walsworth, “High-resolution magnetic resonance spectroscopy using a solid-state spin sensor,” *Nature* **555**, 351–354 (2018).
- [13] D Cohen, T Gefen, L Ortiz, and A Retzker, “Achieving the ultimate precision limit with a weakly interacting quantum probe,” *npj Quantum Information* **6**, 83 (2020).
- [14] Nicolas Staudenmaier, Anjusha Vijayakumar-Sreeja, Genko Genov, Daniel Cohen, Christoph Fidler, Johannes Lang, Alex Retzker, Fedor Jelezko, and Santiago Oviedo-Casado, “Optimal Sensing Protocol for Statistically Polarized Nano-NMR with NV Centers,” *Phys. Rev. Lett.* **131**, 150801 (2023).
- [15] Tuvia Gefen, David A Herrera-Martí, and Alex Retzker, “Parameter estimation with efficient photodetectors,” *Physical Review A* **93**, 032133 (2016).
- [16] Martin B Plenio and Susana F Huelga, “Sensing in the presence of an observed environment,” *Physical Review A* **93**, 032123 (2016).
- [17] Meri Harutyunyan, Bruno Peaudecerf, Dominique Sugny, and Stéphane Guérin, “Qubit sensing by optimal narrowband pulses: Demonstration for rabi frequency sensing,” *Physical Review Research* **7**, 043255 (2025).
- [18] Vittorio Giovannetti, Seth Lloyd, and Lorenzo Maccone, “Advances in quantum metrology,” *Nature photonics* **5**, 222–229 (2011).
- [19] Susanna F Huelga, Chiara Macchiavello, Thomas Pellizzari, Artur K Ekert, Martin B Plenio, and J Ignacio Cirac, “Improvement of frequency standards with quantum entanglement,” *Physical Review Letters* **79**, 3865 (1997).
- [20] Rafał Demkowicz-Dobrzański, Jan Kołodyński, and Mădălin Guță, “The elusive heisenberg limit in quantum-enhanced metrology,” *Nature communications* **3**, 1063 (2012).
- [21] Rafał Demkowicz-Dobrzański and Lorenzo Maccone, “Using entanglement against noise in quantum metrology,” *Phys. Rev. Lett.* **113**, 250801 (2014).
- [22] David A Herrera-Martí, Tuvia Gefen, Dorit Aharonov, Nadav Katz, and Alex Retzker, “Quantum error-correction-enhanced magnetometer overcoming the limit imposed by relaxation,” *Physical review letters* **115**, 200501 (2015).
- [23] Pavel Sekatski, Michalis Skotiniotis, Janek Kołodyński, and Wolfgang Dür, “Quantum metrology with full and fast quantum control,” *Quantum* **1**, 27 (2017).
- [24] Rafał Demkowicz-Dobrzański, Jan Czajkowski, and Pavel Sekatski, “Adaptive Quantum Metrology under General Markovian Noise,” *Phys. Rev. X* **7**, 041009 (2017).
- [25] Sisi Zhou, Mengzhen Zhang, John Preskill, and Liang Jiang, “Achieving the Heisenberg limit in quantum metrology using quantum error correction,” *Nat. Commun.* **9**, 78 (2018).
- [26] Yuxiang Yang, “Memory effects in quantum metrology,” *Physical review letters* **123**, 110501 (2019).
- [27] Sisi Zhou and Liang Jiang, “Optimal approximate quantum error correction for quantum metrology,” *Phys. Rev. Research* **2**, 013235 (2020).
- [28] Sisi Zhou and Liang Jiang, “Asymptotic theory of quantum channel estimation,” *PRX Quantum* **2**, 010343 (2021).
- [29] Qiushi Liu, Zihao Hu, Haidong Yuan, and Yuxiang Yang, “Optimal strategies of quantum metrology with a strict hierarchy,”

- Physical Review Letters **130**, 070803 (2023).
- [30] Stanisław Kurdziałek, Wojciech Górecki, Francesco Albarelli, and Rafał Demkowicz-Dobrzański, “Using adaptiveness and causal superpositions against noise in quantum metrology,” *Phys. Rev. Letters* **131**, 090801 (2023).
- [31] Qiushi Liu and Yuxiang Yang, “Efficient tensor networks for control-enhanced quantum metrology,” *Quantum* **8**, 1571 (2024).
- [32] Piotr Dulian, Stanisław Kurdziałek, and Rafał Demkowicz-Dobrzański, “Qmetro++—python optimization package for large scale quantum metrology with customized strategy structures,” arXiv preprint arXiv:2506.16524 (2025).
- [33] Yue Wu, Shimon Kolkowitz, Shruti Puri, and Jeff D. Thompson, “Erasure conversion for fault-tolerant quantum computing in alkaline earth rydberg atom arrays,” *Nature Communications* **13** (2022), 10.1038/s41467-022-32094-6.
- [34] Aleksander Kubica, Arbel Haim, Yotam Vaknin, Harry Levine, Fernando Brandão, and Alex Retzker, “Erasure Qubits: Overcoming the T_1 Limit in Superconducting Circuits,” *Phys. Rev. X* **13**, 041022 (2023).
- [35] Pascal Scholl, Adam L. Shaw, Richard Bing-Shiun Tsai, Ran Finkelstein, Joonhee Choi, and Manuel Endres, “Erasure conversion in a high-fidelity Rydberg quantum simulator,” *Nature* **622**, 273–278 (2023).
- [36] Levine, H., et al., “Demonstrating a Long-Coherence Dual-Rail Erasure Qubit Using Tunable Transmons,” *Phys. Rev. X* **14**, 011051 (2024).
- [37] Matthew N. H. Chow, Vikas Buchemavari, Sivaprasad Omanakuttan, Bethany J. Little, Saurabh Pandey, Ivan H. Deutsch, and Yuan-Yu Jau, “Circuit-based leakage-to-erasure conversion in a neutral-atom quantum processor,” *PRX Quantum* **5**, 040343 (2024).
- [38] James D Teoh, Patrick Winkel, Harshvardhan K Babla, Benjamin J Chapman, Jahan Claes, Stijn J de Graaf, John WO Garmon, William D Kalfus, Yao Lu, Aniket Maiti, et al., “Dual-rail encoding with superconducting cavities,” *Proceedings of the National Academy of Sciences* **120**, e2221736120 (2023).
- [39] Akshay Kootandavida, Ioannis Tsioutsios, Aikaterini Kargioti, Cassidy R Smith, Vidul R Joshi, Wei Dai, James D Teoh, Jacob C Curtis, Luigi Frunzio, Robert J Schoelkopf, et al., “Erasure detection of a dual-rail qubit encoded in a double-post superconducting cavity,” *Physical Review Letters* **132**, 180601 (2024).
- [40] Mingyu Kang, Wesley C Campbell, and Kenneth R Brown, “Quantum error correction with metastable states of trapped ions using erasure conversion,” *PRX Quantum* **4**, 020358 (2023).
- [41] Shuo Ma, Genyue Liu, Pai Peng, Bichen Zhang, Sven Jandura, Jahan Claes, Alex P Burgers, Guido Pupillo, Shruti Puri, and Jeff D Thompson, “High-fidelity gates and mid-circuit erasure conversion in an atomic qubit,” *Nature* **622**, 279–284 (2023).
- [42] Shouzhen Gu, Alex Retzker, and Aleksander Kubica, “Fault-tolerant quantum architectures based on erasure qubits,” *Physical Review Research* **7**, 013249 (2025).
- [43] Shoham Jacoby, Yotam Vaknin, Alex Retzker, and Arne L Grimsmo, “Magic state injection with erasure qubits,” *PRX Quantum* **6**, 040323 (2025).
- [44] Yingkai Ouyang, Nathan Shettell, and Damian Markham, “Robust quantum metrology with explicit symmetric states,” *IEEE Transactions on Information Theory* **68**, 1809–1821 (2021).
- [45] Yingkai Ouyang and Narayanan Rengaswamy, “Describing quantum metrology with erasure errors using weight distributions of classical codes,” *Physical Review A* **107**, 022620 (2023).
- [46] Yao Ma, Mi Pang, Libo Chen, and Wen Yang, “Improving quantum parameter estimation by monitoring quantum trajectories,” *Physical Review A* **99**, 032347 (2019).
- [47] Timm Kielinski, Piet O Schmidt, and Klemens Hammerer, “Ghz protocols enhance frequency metrology despite spontaneous decay,” *Science Advances* **10**, eadr1439 (2024).
- [48] Pradeep Niroula, Jack Dolde, Xin Zheng, Jacob Bringewatt, Adam Ehrenberg, Kevin C. Cox, Jeff Thompson, Michael J. Gullans, Shimon Kolkowitz, and Alexey V. Gorshkov, “Quantum Sensing with Erasure Qubits,” *Phys. Rev. Lett.* **133**, 080801 (2024).
- [49] Hongzhen Chen, Yu Chen, Jing Liu, Zibo Miao, and Haidong Yuan, “Quantum metrology enhanced by leveraging informative noise with error correction,” *Physical Review Letters* **133**, 190801 (2024).
- [50] Shuo Ma, Jonathan Dolde, Xin Zheng, Dhruva Ganapathy, Alexander Shtov, Jenny Chen, Anke Stöltzel, Bennett J Christensen, and Shimon Kolkowitz, “Enhancing optical lattice clock coherence times with erasure conversion,” arXiv preprint arXiv:2505.06437 (2025).
- [51] Cheng-Ju Lin, Zi-Wen Liu, Victor V Albert, and Alexey V Gorshkov, “Covariant quantum error-correcting codes with metrological entanglement advantage,” *Physical Review Letters* **135**, 110801 (2025).
- [52] Masahiro Kitagawa and Masahito Ueda, “Squeezed spin states,” *Physical Review A* **47**, 5138 (1993).
- [53] Carl W. Helstrom, “Quantum detection and estimation theory,” *Journal of Statistical Physics* **1**, 231–252 (1969).
- [54] Samuel L Braunstein and Carlton M Caves, “Statistical distance and the geometry of quantum states,” *Phys. Rev. Lett.* **72**, 3439 (1994).
- [55] K. Maciejszczak, Quantum fisher information: Variational principle and simple iterative algorithm for its efficient computation (2013), “arxiv:1312.1356 [quant-ph],” .
- [56] Árpád Lukács, Róbert Trényi, Tamás Vértesi, and Géza Tóth, “Iterative optimization in quantum metrology and entanglement theory using semidefinite programming,” *Quantum Science and Technology* **11**, 015042 (2026).
- [57] Lewis A Clark, Adam Stokes, and Almut Beige, “Quantum jump metrology,” *Physical Review A* **99**, 022102 (2019).
- [58] Dayou Yang, Susana F Huelga, and Martin B Plenio, “Efficient information retrieval for sensing via continuous measurement,” *Physical Review X* **13**, 031012 (2023).
- [59] Marco Radaelli, Joseph A Smiga, Gabriel T Landi, and Felix C Binder, “Parameter estimation for quantum jump unraveling,” *Quantum* **10**, 1993 (2026).

- [60] See the Supplemental Material.
- [61] Jan Kolodyński and Rafał Demkowicz-Dobrzański, “Efficient tools for quantum metrology with uncorrelated noise,” *New J. Phys.* **15**, 073043 (2013).
- [62] Akio Fujiwara and Hiroshi Imai, “A fibre bundle over manifolds of quantum channels and its application to quantum statistics,” *J. Phys. A* **41**, 255304 (2008).
- [63] Rafał Demkowicz-Dobrzański, Marcin Jarzyna, and Jan Kołodyński, “Quantum limits in optical interferometry,” *Progress in Optics* **60**, 345–435 (2015).
- [64] For thermal noise with $G = \sigma_x$ and decay and excitation rates of γ_2, γ_1 , the bound is $\mathfrak{J}^{(\text{ult})} = \frac{4NT}{\gamma_1 + \gamma_2}$. [23].
- [65] Pavel Sekatski and Martí Perarnau-Llobet, “Optimal nonequilibrium thermometry in markovian environments,” *Quantum* **6**, 869 (2022).
- [66] James W Gardner, Simon A Haine, Joseph J Hope, Yanbei Chen, and Tuvia Gefen, “Lindblad estimation with fast and precise quantum control,” *Physical Review Applied* **24**, 044055 (2025).
- [67] Luca Pezze, Augusto Smerzi, Markus K Oberthaler, Roman Schmied, and Philipp Treutlein, “Quantum metrology with nonclassical states of atomic ensembles,” *Rev. Mod. Phys.* **90**, 035005 (2018).
- [68] Jan Kołodyński and Rafał Demkowicz-Dobrzański, “Efficient tools for quantum metrology with uncorrelated noise,” *New J. Phys.* **15**, 073043 (2013).
- [69] Florentin Reiter and Anders S. Sørensen, “Effective operator formalism for open quantum systems,” *Phys. Rev. A* **85**, 032111 (2012).
- [70] R. Azouit, A. Sarlette, and P. Rouchon, “Adiabatic elimination for open quantum systems with effective lindblad master equations,” in *2016 IEEE 55th Conference on Decision and Control (CDC)* (2016) pp. 4559–4565.
- [71] Jérémie Guillaud, Joachim Cohen, and Mazyar Mirrahimi, “Quantum computation with cat qubits,” *SciPost Phys. Lect. Notes*, 72 (2023).
- [72] Sheldon M Ross, *Stochastic processes* (John Wiley & Sons, 1995).